

DOE/NASA/4105-4
NASA CR-182248

1N-44
217214
4

NASA Lewis Stirling Engine Computer Code Evaluation

Timothy J. Sullivan
Sverdrup Technology, Inc.
NASA Lewis Research Center Group

January 1989

(NASA-CR-182248) NASA LEWIS STIRLING ENGINE
COMPUTER CODE EVALUATION Final Report
(Sverdrup Technology) 43 p

N89-24741

Unclas
G3/44 0217214

Prepared for
NATIONAL AERONAUTICS AND SPACE ADMINISTRATION
Lewis Research Center
Under Contract NAS3-24105

for

U.S. DEPARTMENT OF ENERGY
Conservation and Renewable Energy
Office of Vehicle and Engine R&D

DISCLAIMER

This report was prepared as an account of work sponsored by an agency of the United States Government. Neither the United States Government nor any agency thereof, nor any of their employees, makes any warranty, express or implied, or assumes any legal liability or responsibility for the accuracy, completeness, or usefulness of any information, apparatus, product, or process disclosed, or represents that its use would not infringe privately owned rights. Reference herein to any specific commercial product, process, or service by trade name, trademark, manufacturer, or otherwise, does not necessarily constitute or imply its endorsement, recommendation, or favoring by the United States Government or any agency thereof. The views and opinions of authors expressed herein do not necessarily state or reflect those of the United States Government or any agency thereof.

Printed in the United States of America

Available from

National Technical Information Service
U.S. Department of Commerce
5285 Port Royal Road
Springfield, VA 22161

NTIS price codes¹

Printed copy: A02

Microfiche copy: A01

¹Codes are used for pricing all publications. The code is determined by the number of pages in the publication. Information pertaining to the pricing codes can be found in the current issues of the following publications, which are generally available in most libraries: *Energy Research Abstracts (ERA)*; *Government Reports Announcements and Index (GRA and I)*; *Scientific and Technical Abstract Reports (STAR)*; and publication, NTIS-PR-360 available from NTIS at the above address.

NASA Lewis Stirling Engine Computer Code Evaluation

Timothy J. Sullivan
Sverdrup Technology, Inc.
NASA Lewis Research Center Group

January 1989

Prepared for
National Aeronautics and Space Administration
Lewis Research Center
Cleveland, Ohio 44135
Under Contract NAS3-24105

for
U.S. DEPARTMENT OF ENERGY
Conservation and Renewable Energy
Office of Vehicle and Engine R&D
Washington, D.C. 20545
Under Interagency Agreement DE-AI01-85CE50112

NASA LEWIS STIRLING ENGINE COMPUTER CODE EVALUATION

Timothy J. Sullivan
Sverdrup Technology, Inc.
NASA Lewis Research Center Group
Cleveland, Ohio 44135

SUMMARY

In support of the U.S. Department of Energy's Stirling Engine Highway Vehicle Systems program, the NASA Lewis Stirling engine nodal-analysis performance code was evaluated by comparing code predictions without engine-specific calibration factors to Stirling engine test data. Stirling engine test data was obtained from the GPU-3, P-40, and RE-1000 Stirling engines, over a wide range of operating conditions. The code evaluation process included: an investigation of prediction error trends for changes in the operating conditions, an investigation into the cause of the power prediction errors, and an evaluation of the possible computer model shortcomings.

The error in predicting power output was -11 percent for the P-40 and 12 percent for the RE-1000 at design conditions and 16 percent for the GPU-3 at near-design conditions (2000 rpm engine speed versus 3000 rpm at design). The efficiency and heat rate predictions showed better agreement with engine test data than did the power predictions. Concerning all data points, the GPU-3 prediction errors were much greater than those for the P-40 or RE-1000. The GPU-3 power error significantly increased with decreasing power level and when using helium working fluid (compared to hydrogen).

The error in predicting the GPU-3 brake power was mainly a result of inaccuracy in predicting the pressure phase angle. The RE-1000 indicated power prediction error was mainly a result of inaccuracy in predicting the pressure amplitude. The analysis of P-40 performance prediction errors with respect to pressure amplitude and phasing was difficult because of relatively large errors in measuring the working-fluid pressure phase angle.

Analysis into the GPU-3 pressure phase angle prediction error suggested that improvements to the hysteresis loss model could have a significant effect on overall Stirling engine performance predictions. Improvements in predicting other loss mechanisms such as gas leakage by the pistons, effects of oscillating flow on pressure drops and heat transfer, and appendix gap losses will undoubtedly improve performance predictions as well.

INTRODUCTION

This study was done in support of the U.S. Department of Energy (DOE) Stirling Engine Highway Vehicle Systems program. The NASA Lewis Research Center, through interagency agreement DE-AI01-85CE50112 with DOE, is responsible for management of the project under the program direction of the DOE Office of Transportation Systems, Heat Engine Propulsion Division.

This report deals with the evaluation of the NASA Lewis Stirling engine nodal-analysis performance code. This study was completed by comparing code predictions to Stirling engine test data. The objectives for this evaluation

were (1) to determine the extent of agreement of the computer model with a wide range of Stirling engine test data from a variety of engines, using no engine-specific calibration factors and (2) to identify shortcomings of the model.

The Stirling engine computer model, described in reference 1, is a nodal-analysis, time marching simulation. This thermodynamic performance code is designed for simulating engine performance under steady periodic operating conditions.

The simulation of Stirling engine performance is difficult because common simplifying assumptions can't be made when dealing with the working fluid dynamics. The fluid flow is unsteady, compressible, mainly turbulent, and multidimensional, with varying properties. With the present state of the art on modeling these complex flows, the complete solution to the governing equations would require a large amount of computer time (on a "supercomputer"). The alternative is to make simplifying assumptions and test the validity of those assumptions by comparing the computer model predictions with test data.

In the past, efforts have been made to validate the NASA Lewis Stirling engine computer model. Tew (ref. 2) compared and calibrated single-cylinder Stirling engine computer model predictions with test results. Tew found that code predictions could be improved by increasing the pressure drop prediction. Allen (ref. 3) compared test results of a 40-kW Stirling engine to computer model predictions and speculated that the over predictions in brake power were caused by piston-seal leakage not being accounted for in the computer model.

Free-piston Stirling engine computer model predictions from the NASA Lewis code were compared to test data by Tew (ref. 4). The performance prediction error was decreased by mainly increasing the predicted pressure drop and decreasing the displacer gas-spring leakage factor. Geng (ref. 5) calibrated a slightly different version of the free-piston Stirling engine computer model. Large increases in the expansion and compression-space heat transfer coefficients were found to improve performance predictions.

The code evaluation process reported here used engine test data that represented a wide range of operating conditions, for different types of Stirling engines. All engine test data was collected at NASA Lewis. The Stirling engines used for this study were the GPU-3, P-40, and RE-1000. The GPU-3 is a 6-kW single-cylinder, rhombic-drive Stirling engine, described in reference 6. The P-40 is a 40-kW four-cylinder double-acting Stirling engine, described in reference 7. The RE-1000 is a 1-kW single-cylinder free-piston Stirling engine, described in reference 8. A variable-stroke Stirling engine, the Advenco, was initially included in this study; however, because of the uncertainty in the mechanical loss, reasonable comparisons with the test data could not be completed.

Predictions were then made with the computer model using operating conditions identical to those used in the test cell. Predicted and actual engine performance were then compared and analyzed. The evaluation of the Stirling engine computer model included: an investigation of prediction error trends for changes in operating conditions, a summary of Stirling engine prediction errors, and investigation into the cause of the power prediction errors, and finally an evaluation of the possible computer model "shortcomings".

PROCEDURE AND ANALYSIS

Description of Stirling Engine Computer Model

The NASA Lewis Stirling engine computer model is a nodal-analysis, time marching simulation. The nodes, or control volumes, are used to simplify the solution of the governing equations, for each time step. Reference 1 describes the code, which was initially designed for predicting steady periodic performance for a kinematic Stirling engine.

The NASA Stirling engine computer model has been modified by both Mechanical Technology Incorporated (ref. 9) and Tew, of NASA, (ref. 4) to model the free-piston Stirling engine. The thermodynamics of the free-piston Stirling engine are similar to that for the kinematic Stirling engine. The free-piston Stirling engine does not couple the displacer and piston mechanically; rather, the motion of the displacer and piston is governed by working fluid and gas-spring pressure forces. The displacer and piston gas springs and gas leakage paths are accounted for in the free-piston Stirling engine simulation.

The free-piston version of the NASA Lewis Stirling engine computer model was improved by Geng (ref. 5). Notable improvements were made in the cooler heat exchanger model, gas leakage model, and displacer gas-spring model. Sullivan (the author of this report) also made various improvements to the kinematic version of the computer model. Major improvements, over that presented in reference 4, were made in the regenerator heat exchanger model and the overall flow-path pressure drop model. Improvements to the overall flow-path pressure drop model are described in reference 10.

Prior to evaluating the computer model, engine-specific calibration factors that were used to force code predictions to agree with engine test data were removed. The removal of these calibration factors was necessary for an unbiased evaluation of the computer model.

A list of possible computer model shortcomings was made prior to the comparisons. These possible shortcomings are as follows:

- (1) Auxiliary and mechanical loss uncertainty
- (2) Inadequate or no gas leakage loss model
- (3) Primitive appendix gap (displacer-cylinder gap) loss model
- (4) Inadequate hysteresis (cylinder heat transfer) loss model
- (5) Use of steady flow friction factor and heat transfer coefficient correlations (as well as 1-D fluid flow approximation)
- (6) Simplified treatment of the momentum equation and energy equation
- (7) Finite number of nodes and increments per cycle

The importance of these computer model shortcomings was readdressed when analyzing results from this study.

Experimental Stirling Engine Testing

The Ground Power Unit (GPU) Stirling engine was built by the General Motors Research Laboratory; it is referred to as the GPU-3 since it was meant to deliver 3 kW of electrical energy from the unit as a whole. The GPU-3 is a 6-kW, single-cylinder, rhombic-drive Stirling engine, described in reference 6 and pictured in figure 1. The GPU-3 test data used in this study included a

range of average heater-tube gas temperatures, mean working-space gas pressures, and engine speeds with both helium and hydrogen working fluids. Engine testing details are given in references 6 and 11. GPU-3 design operating conditions are given in table I.

The P-40 Stirling engine was built by United Stirling of Sweden. The P-40 is a 40-kW, double-acting, four-cylinder Stirling engine, described in reference 7 and shown in figure 2. The P-40 test data used in this study was for a range of mean working-space gas pressure and engine speeds. The working fluid was hydrogen and the average heater-tube wall temperature was held fixed. Further P-40 testing details are in reference 3. Engine design operating conditions are shown in table I.

The RE-1000 free-piston Stirling engine was built by Sunpower, Inc. The RE-1000 is a single cylinder Stirling engine capable fo 1-kW output and is described in reference 8 and shown in figure 3. The engine test data was collected using a dashpot load, for a range of piston strokes, mean working-space gas pressures, average heater-tube wall temperatures, and average coolant inlet temperatures. Details of the engine testing are in reference 12. The working fluid was helium. RE-1000 design operating conditions are shown in table I.

The GPU-3, P-40, and RE-1000 Stirling engine dimensions are listed in tables A.I, A.II, A.III, and A.IV of appendix A. The engine test data that were used in this study are shown in tables B.I, B.II, B.III of appendix B. All engine test data were taken at NASA Lewis.

Stirling Engine Performance Predictions

Necessary inputs to the computer model are defined in table II. Space and time increment specifications for the computer model were chosen to result in a predicted error in the energy balance of roughly 1 percent or less. Code options used for this study included: working fluid was modeling using real properties (instead of ideal); average heater-tube wall temperature was input for the P-40 and RE-1000, and heater-tube gas temperature was input for the GPU-3. Also the RE-1000 piston and displacer motions were input to the computer model.

The Stirling engine operating conditions that were used in the computer model matched those for the experimental engine testing. The mean gas pressure input to the model was the experimental mean compression-space gas pressure. Various heater-tube wall (or heater-tube gas) temperature mean compression-space gas pressure. Various heater-tube wall (or heater-tube gas) temperature measurements were spatially averaged and input into the computer model. Also averaged were various engine component temperatures, such as cylinder wall temperature (used for conduction calculations).

The GPU-3 averaged heater-tube gas temperature was the average temperature measurement from three thermocouples, each located inside a separate heater tube. Two heater-tube wall temperatures were input for the P-40 simulation: one to represent the heater-tubes in the back row and one to represent the heater-tubes in the front row. These two-heater-tube wall temperatures were based on a total of twelve thermocouple readings with the thermocouples located at various locations along the outside heater-tube wall. The P-40 heater-tube thermocouples were mounted on the coolest surface (circumferentially) of the

heater tube so corrections had to be made to these readings to obtain an average (circumferentially) tube temperature. These corrections depended on the fuel flow rate and were based on data from United Stirling of Sweden. The RE-1000 average heater-tube wall temperature was an average of twelve thermocouple readings.

Indicated power was used for the RE-1000 prediction-experimental comparison; brake power was used for the GPU-3 and P-40 comparison. The GPU-3 and P-40 heat inputs were defined as the energy input from the fuel minus the burner losses (the burner losses were calculated from energy balances). The RE-1000 heater tubes were electrical conductors; the heat input was defined as the voltage drop across the heater tubes times the current.

Throughout this report the term "pressure amplitude" was redefined to be the difference between the maximum gas pressure and minimum gas pressure. Normally the gas pressure amplitude is defined as maximum minus the mean gas pressure.

Use of the Pressure-Wave Curve-Fit (PWCF) Code

Prediction errors for the power output and heat input depend on the gas-pressure-wave amplitude (pressure amplitude) error, the gas-pressure-wave/piston-position phase angle (pressure phase angle) error, and the mechanical loss error (when considering the brake power prediction error). The power output and heat input prediction errors also depend on any error in simulating the engine volume variations, but the simulated volume variations used for this study were considered perfectly accurate.

It was desired to determine which pressure parameter prediction error (amplitude or phase angle) was responsible for the power output and heat input prediction errors; attention was also given to the effect of a mechanical loss error. Due to the nature of the NASA Lewis Stirling engine computer simulation, it is unable to perform this type of investigation. Thus, the PWCF code was written for this purpose. PWCF stands for Pressure-Wave Curve-Fit Integrator and a detailed description of the PWCF code can be found in appendix C.

The following procedure was used to investigate Stirling engine performance sensitivity to prediction errors in the pressure parameters:

(1) Input experimental pressure parameters (both amplitude and phase angle) to the PWCF code and calculate performance.

(2) Calculate performance again, now substituting either the predicted pressure amplitude or the predicted phase angle.

(3) Compare the two calculated performances to determine the effect of the difference between the predicted and the measured pressure amplitude or phase angle.

Note from appendix C that the calculations from the PWCF code for brake power agree well with predictions from the NASA Lewis Stirling engine computer simulation. However, agreement for the heat input was not acceptable and thus, the PWCF code could not be used to analyze errors in heat input.

RESULTS AND DISCUSSION

This section covers the following: investigation of trends in prediction errors for each Stirling engine, summary of Stirling engine prediction errors, investigation into the effects of pressure amplitude and phasing on the power output prediction errors, and evaluation of the computer model shortcomings. Throughout this report the prediction "error" refers to an error based on percentages and is defined as the predicted value minus the experimental value divided by the experimental value. The prediction error trends discussed below considered all operating conditions for each Stirling engine and are accompanied with representative figures showing the trends.

Comparisons for the GPU-3 Stirling Engine

The following GPU-3 operating conditions were varied: engine speed, mean compression-space gas pressure, average heater-tube gas temperature, and working fluid. Design operating conditions are shown in table I. The coolant inlet temperature was held constant at 20 °C for all GPU-3 data points used in this study. Brake power versus engine speed, for a fixed heater-tube gas temperature and mean pressure, is shown in figure 4. Brake power is seen to be overpredicted. The error in predicting brake power increases with engine speed and is larger when the working fluid is helium. Figure 5 shows brake power versus engine speed, for various mean pressures. The working fluid is helium and the heater-tube gas temperature is held fixed. The brake power prediction error (remember this is a percentage error) decreases with increasing mean pressure; similar results occurred when using hydrogen working fluid. Brake power variation with engine speed and heater-tube gas temperature is shown in figure 6. The effect of the heater-tube gas temperature on the brake power prediction error is considered insignificant.

Heat input versus engine speed for hydrogen and helium working fluids is shown in figure 7. The heater-tube gas temperature and mean pressure are held fixed. Heat input is over predicted for both gases. Figure 8 shows heat input versus engine speed, for a variation in mean pressure for helium working fluid. The error in predicting heat input is relatively insensitive to changes in the engine speed and mean pressure. Figure 9 shows heat input for variations in the engine speed and heater-tube gas temperature. The mean pressure is held fixed and the working fluid is hydrogen; the results are similar when using helium working fluid. Notice the prediction error increases as the heater-tube gas temperature rises.

The compression-space pressure amplitude versus engine speed, for various heater-tube gas temperatures and for hydrogen working fluid, is shown in figure 10; remember the pressure amplitude is defined as the maximum pressure minus the minimum pressure. Notice that the error increases with the heater-tube gas temperature. The prediction error proved to be insensitive to mean pressure. These trends are about the same for the expansion-space gas pressure amplitude as well as when using helium working fluid. The absolute prediction error was greater for helium working fluid than for hydrogen. Although the pressure amplitude error is insensitive to mean pressure and relatively insensitive to engine speed, the GPU-3 brake power error depends on pressure and increases with engine speed; this suggests that the GPU-3 brake power error is not a result of inaccuracy in the prediction of the pressure amplitude.

Comparisons for the P-40 Stirling Engine

Variations in the P-40 engine operating conditions were accomplished by changing the mean gas pressure and the engine speed. The working fluid was hydrogen for all P-40 tests. P-40 design operating conditions are shown in table I. Figure 11 shows brake power versus engine speed, for variations in mean pressure. Brake power is underpredicted with the error increasing slightly with increasing engine speed and decreasing slightly with increasing mean pressure; these variations in the P-40 brake power prediction error are significantly smaller than those for the GPU-3. Allen's comparison of code predictions to engine test data (ref. 3) showed that P-40 brake power was slightly overpredicted. Prior to this study, the dead volumes that were input to the computer model were updated based on recent engine measurements. This improvement caused the change in P-40 predictions relative to Allen's comparison.

Heat input versus engine speed, for various mean pressures, is shown in figure 12. Heat input agreement is very good with no apparent trends in the prediction error (percentage error). Figure 13 shows the compression-space pressure amplitude versus engine speed, for various mean pressures. The agreement again is very good with respect to both engine speed and mean pressure.

Comparisons for the RE-1000 Stirling Engine

The following RE-1000 operating conditions were varied: piston stroke, mean gas pressure, average heater wall temperature, and coolant inlet temperature; while one of these parameters was varied, the other three were held at design conditions. Engine design operating conditions are shown in table I. The working fluid is helium. Measurement error bands are shown on the figures.

Indicated power versus piston stroke is shown in figure 14. Indicated power is over predicted with the prediction error increasing with piston stroke. Figures 15 and 16 show indicated power versus mean pressure and heater wall temperature, respectively. The indicated power prediction error decreases with mean pressure and increases with heater wall temperature. Indicated power versus coolant inlet temperature is shown in figure 17. The error decreases with increasing coolant inlet temperature. These variations in the RE-1000 indicated power prediction error are significantly smaller than those for the GPU-3.

Heat input versus piston stroke is shown in figure 18. Figures 19 and 20 show heat input versus mean pressure and heater wall temperature, respectively. Heat input versus coolant inlet temperature is shown in figure 21. Considering all data points, the error in predicting heat input can be considered insensitive to variations in all four parameters.

Compression-space pressure amplitude versus heater wall temperature is shown in figure 22. The error increases with increasing heater wall temperature. Considering a variation in all the independent parameters, a variation in the heater wall temperature had the biggest effect on the prediction error in the compression-space amplitude.

Summary of Stirling Engine Prediction Errors

Engine performance prediction errors for design (or near-design) and low power conditions, are shown in table III. Two low power conditions are shown for the RE-1000, at low piston stroke and at low mean gas pressure. For each engine, the errors for the low power condition shown are typical of other low power condition errors, not shown on the table.

The GPU-3 power error is the largest, when comparing errors of all engines. The GPU-3 error is larger with helium working fluid than with hydrogen and also when decreasing the power level. The efficiency prediction generally shows better agreement to engine test data than does the power prediction. This is due to the value of the heat input prediction error. The heat input and heat out of the engine errors are generally lower than the power prediction errors; they are generally larger for the GPU-3 engine, when compared to the other engines. When compared to the power errors, these errors in heat input and heat out are relatively insensitive to power level.

The errors in gas temperature were based on time-averaged gas temperatures. The predicted gas temperatures for the GPU-3 and RE-1000 engines compare well with the test data; the prediction errors for the P-40 are larger.

For each engine, the errors in the expansion and compression-space pressure amplitudes are lower than the power errors. The GPU-3 pressure amplitude errors are significantly lower than the power errors; this seems to suggest that the error in predicting the pressure amplitude is not responsible for the GPU-3 power prediction error. The P-40 pressure amplitudes are over predicted. The maximum and minimum P-40 gas pressures, used to determine the pressure amplitudes, were measured (with large strain gage transducers) in the P-40 vent and pressurization lines, respectively; these pressure amplitude measurements are considered sufficiently accurate. The fact that the P-40 pressure amplitudes are over predicted and the P-40 brake power is under predicted suggests an inconsistency, which will be discussed later in this report.

The absolute error in the compression-space pressure phase angle is seen to be relatively large for the GPU-3 and negligible for the RE-1000. The GPU-3 phase angle absolute errors are approximate because of uncertainty in the measurement of the actual engine pressure phase angle. The heat exchanger pressure-drop amplitude was measured on the RE-1000 engine; the pressure-drop amplitude prediction errors are large.

Pressure Parameters Effects on Power Prediction Errors

The investigation into the power prediction errors was accomplished by using the PWCF code, described in the PROCEDURE AND ANALYSIS section and in appendix C. Prior to using the PWCF code for the GPU-3 and P-40 engines, the accuracy of the mechanical loss model input to the code had to be considered. The GPU-3 brake power prediction error may have been caused by a large under-prediction in the mechanical loss. The mechanical loss used for the GPU-3 predictions was derived from experimental data for the energy balance. The mechanical loss was considered to be the sum of the heat rejected to the oil and the buffer-space cooling water (ref. 11). An attempt was also made to measure the mechanical loss more directly by doing "motoring tests" (ref. 11).

The mechanical loss derived from the motoring test was considered to be an upperbound for the true GPU-3 mechanical loss.

Figure 23 shows the effect that this motoring test data has on the brake power prediction compared to the baseline prediction (using the energy balance mechanical loss). Analysis of all GPU-3 data showed that, when using the motoring test mechanical loss for hydrogen working fluid, the prediction error decreased by an average of 18 percent at low engine speeds and 60 percent at high engine speeds. When helium working fluid was used, the use of the motoring test mechanical loss resulted in the prediction error increasing by an average of 11 percent at low speeds and decreasing by an average of 30 percent at high engine speeds.

Using the PWCF code, figure 24 shows the effect on brake power due to the prediction error in the pressure amplitude or pressure phase angle, for various operating conditions. The error in predicting the GPU-3 brake power was primarily accounted for by a phase angle prediction error. Similar results were seen for hydrogen working fluid. Tew (ref. 2) found that GPU-3 performance prediction accuracy could be greatly improved by increasing the regenerator pressure drop by a factor of four for helium working fluid. However, increasing the predicted GPU-3 regenerator pressure drop, which accounts for the majority of the flow path pressure drop, resulted in a negligible change in the pressure phase angle. Therefore, inaccuracy in the regenerator pressure-drop prediction (or entire working space pressure-drop prediction) does not account for the poor predictions in the GPU-3 brake power as it doesn't improve the agreement for the pressure phase angle.

The use of measured P-40 pressure parameters in the PWCF code produced a value for indicated power that was below the measured value of brake power. The P-40 pressure phase angles were measured using miniature, dynamic, strain gage pressure transducers. Because the P-40 pressure amplitude is considered to be accurately measured, the measured P-40 pressure phase angles must have been in error. Using the PWCF code, the pressure phase angle measurement error was estimated equal to -7° . Two main problems plagued the measurement of the P-40 gas pressure phase angle: uncertainty of the crank angle and sensitivity errors of the miniature, dynamic, strain gage pressure transducers. Allen's (ref. 3) speculation that the inaccuracy in the predicted P-40 brake power was caused by not modeling the piston-seal leakage was based on the dynamic pressure measurement and thus, this speculation may be incorrect.

An examination of error trends based on the power measurements and the pressure amplitude measurements (based on measurements of maximum and minimum pressures) may lead to a better understanding of the P-40 brake power prediction error. The P-40 brake power prediction error increased slightly with increasing engine speed, yet the pressure amplitude error was insensitive to variations in engine speed. This seems to suggest that the brake power error is attributed to an error in predicting the pressure phase angle.

Using the results of the PWCF code, figure 25 shows the effect of the RE-1000 indicated power due to the error in the pressure amplitude or pressure phase angle, for various operating conditions. The error in predicting the indicated power was primarily accounted for by the pressure amplitude prediction error.

Evaluation of Computer Model Shortcomings

Sensitivity to computer model precision - Computer model precision was varied to determine its effect on the Stirling engine performance prediction error. Computer model parameters were altered to obtain a "high precision" computer model. Then these predictions were compared to predictions from the "standard" computer model, for all three engines at design conditions. Alterations to the code were as follows: number of heat exchanger control volumes, number of time increments per cycle, and the number of engine cycles were increased to their asymptotic limit. The number of heat exchanger control volumes was increased from 3 to 25 (per heat exchanger). The number of increments per cycle was increased from 360 to 900 and the number of engine cycles was increased from 30 to 100. Also, "two passes" through the calculations were made, which approximately coupled the momentum and energy equations.

Increasing the computer model precision from "standard" precision to "high" precision resulted in a slight increase in the predicted power and a slight decrease in heat input and heat-out predictions. The increase of computer model precision caused the GPU-3 and RE-1000 power prediction errors to increase; therefore, increasing the computer model precision does not account for the observed performance prediction errors.

Parameters that effect the pressure phase angle - The largest power prediction error occurred for the GPU-3 and was caused primarily by inaccuracy in predicting the pressure phase angle. For the GPU-3, the maximum gas pressure occurred at approximately 300°, but is predicted at 312°. Using the Equation of State and assuming that gas pressure is a function of time only:

$$dP = -P \frac{dV}{V} + \frac{R}{V} \sum (T_i dM_i) + \frac{R}{V} \sum (M_i dT_i)$$

where P is gas pressure, V is engine volume, R is gas constant, T_i is gas temperature in i^{th} control volume in engine, and M_i is mass of gas in i^{th} control volume.

When the pressure wave reaches a maximum or minimum, $dP = 0$; at these points,

$$P \frac{dV}{V} = \frac{R}{V} \sum (T_i dM_i) + \frac{R}{V} \sum (M_i dT_i)$$

The two sides of this equation are plotted in figure 26; the curves shown were calculated with the computer model for the GPU-3 Stirling engine at the indicated conditions. For these operating conditions, the computer model predicted $dP = 0$ (maximum gas pressure) at 312°. Notice that the curves cross at approximately 312°; this agreement with the crank angle at which the maximum pressure occurs offers confidence in the above "pressure variation" equation. In order for the predicted pressure phase angle to agree with the measured value, the curves should cross at approximately 300°. If the

$$P \frac{dV}{V}$$

curve were to rise, P would have to increase by a factor of approximately 3 (assuming that the volumes and volume variations are correct); the magnitude of P could not be in error by a factor of 3. Thus, the

$$\frac{R}{V} \sum (T_i dM_i) + \frac{R}{V} \sum (M_i dT_i)$$

terms will have to decrease by a factor of 3.

From an "order of magnitude" analysis,

$$\frac{R}{V} \sum (T_i dM_i) + \frac{R}{V} \sum (M_i dT_i)$$

simplifies to

$$\frac{R}{V} (T_e dM_e + T_c dM_c + M_h dT_h)$$

where subscripts e denotes expansion-space, c denotes compression-space, and h denotes hot side of the engine. Thus, the error in predicting the GPU-3 pressure phase angle is primarily due to an error in predicting dM_e , dM_c , or dT_h .

Relationship of dM_e , dM_c , and dT_h to computer model shortcomings -

Smith (ref. 13) suggested that the temperature difference between the gas and the wall in the cylinder and the heat transfer rate (hysteresis loss) should be out of phase. In the NASA Lewis Stirling engine computer model, the gas-wall temperature difference and the heat transfer rate are modeled with no phase difference. If the predicted cylinder heat transfer was not modeled in phase with the gas-wall temperature difference, the points of maximum and minimum heat transfer would shift to different crank angles. This shift in the cylinder heat transfer wave would have an effect on the phasing of the cylinder gas temperature wave resulting in a variation in dT_h ; this could cause the two curves of figure 26 to intersect at a point near a crank angle of 300°. Improving the accuracy of the hysteresis loss model may improve the GPU-3 pressure phase angle prediction, which in turn will improve the GPU-3 performance prediction accuracy.

Geng (ref. 5) found that increasing the heat transfer coefficient in the expansion and compression spaces improved RE-1000 performance predictions. The expansion-space heat transfer coefficient was increased by a factor of 230; the compression-space heat transfer coefficient was increased by a factor of 50. These variations resulted in a reduction in the gas temperature amplitude, which reduced the predicted pressure amplitude (while the pressure phase angle changed by only 0.2°). The reduction of the pressure amplitude caused the error in predicting the indicated power to be reduced from 12 to 3 percent. In this author's study, the pressure amplitude error was found to be mainly responsible for the error in predicting the RE-1000 indicated power.

This author increased the predicted heat transfer coefficients for the GPU-3 by the same amount as Geng had. The effect on predicted performance was different than that observed by Geng. For the GPU-3, the phase angle of the gas temperature changed (the temperature amplitude was insensitive), resulting in a variation in dT_h . The error in predicting the pressure phase angle was consequently reduced, which resulted in the brake power prediction error being reduced from 16 to 12 percent. Earlier, this investigation showed that the primary reason for the GPU-3 brake power error was inaccuracy in predicting the

pressure phase angle. Note that increasing the cylinder heat transfer coefficient improved the prediction accuracy for the appropriate pressure parameter for each engine (pressure amplitude for the RE-1000, pressure phase angle for the GPU-3), which in turn decreased the error in predicting power. This seems to support the speculation that inaccuracy in the hysteresis loss model accounts for at least part of the Stirling engine prediction error.

Another possible error was inaccuracy in predicting dM_e and dM_c . Gas leakage past the displacer and piston seals would relate to the prediction of dM_e and dM_c . This gas leakage is grossly accounted for in the GPU-3 model and not accounted for in either the P-40 or RE-1000 models. Therefore, the gas leakage model also needs to be addressed, but it is not known what effect this improvement will have on overall performance predictions.

Computer model shortcomings revisited - The list of possible computer model shortcomings was introduced in the PROCEDURE AND ANALYSIS section. From this investigation, we know:

(1) Auxiliary and mechanical loss - Uncertainty does not account for the majority of the Stirling engine performance prediction error with the possible exception of the high-speed points for the GPU-3.

(2) Gas leakage loss model - Inaccuracy in the gas leakage loss model may have a significant effect on the Stirling engine performance prediction error.

(3) Appendix gap loss model - Significance of possible inaccuracy was not evaluated and is still unknown.

(4) Hysteresis loss model - Inaccuracy in the hysteresis loss model may have a significant effect on the Stirling engine performance prediction error.

(5) Friction factor and heat transfer coefficient correlations - Significance of possible inaccuracy was not evaluated and is still unknown (referring to steady flow and 1-D assumptions).

(6) Momentum and energy equations - Numerical treatment of these equations does not account for the majority of the Stirling engine performance prediction error for the engines considered.

(7) Number of nodes and increments per cycle - Approximations due to using the standard number of nodes and time increments per cycle does not result in a significant error in predicting Stirling engine performance.

SUMMARY OF RESULTS

The major results from the evaluation of the NASA Lewis Stirling engine computer simulation are presented below. Computer model predictions were compared to Stirling engine test data for the GPU-3, P-40, and RE-1000 Stirling engines.

1. The error in predicting power at design* conditions was 16 percent for the GPU-3, -11 percent for the P-40, and 12 percent for the RE-1000. The GPU-3

*Near-design conditions for the GPU-3.

error significantly increased with decreasing power level or when using helium as the working fluid instead of hydrogen.

2. The efficiency, heat input, and heat out of the engine predictions generally showed better agreement with engine test data than did the power prediction.

3. The percentage errors in the GPU-3 and P-40 brake power predictions increased with increasing engine speed and decreasing mean gas pressure; the brake power prediction error was attributed to an inaccuracy in predicting the pressure phase angle.

4. The percentage error in the RE-1000 indicated power prediction was attributed to an error in predicting the pressure amplitude.

5. The average gas temperatures had negligible prediction errors for the GPU-3 and RE-1000; the errors in predicting the average gas temperature were larger for the P-40.

6. The computer model precision in terms of the number of nodes, cycles, and time increments per cycle was not a significant factor in the difference between predictions and test data.

7. For the GPU-3, increasing the cylinder heat transfer coefficients resulted mainly in a correction to the pressure phase angle prediction. For the RE-1000, the same change resulted in a correction to the pressure amplitude prediction. The increased accuracy in predicting the GPU-3 pressure phase angle and the RE-1000 pressure amplitude reduced the power prediction errors for both engines.

CONCLUSIONS

The main objective of this study was to compare predictions from the NASA Lewis Stirling engine performance code to Stirling engine test data, for a variety of Stirling engines using no engine-specific calibration factors. Then, analyze these differences to try to determine shortcomings in the computer model.

The engines used for this study were the GPU-3, P-40, and RE-1000. The error in predicting the GPU-3 brake power was a result of the inaccuracy in predicting the working fluid's pressure phase angle; the pressure phase angle is the pressure phasing with respect to the piston position. The error in predicting the RE-1000 indicated power was determined to be a result of inaccuracy in predicting the gas pressure amplitude.

In doing this study, a relatively large measurement error was detected in the P-40 pressure phase angle. The pressure phase angle could not be used in the analysis and thus an accurate understanding of the P-40 prediction discrepancy was impossible. The required level of measurement accuracy needs to be carefully considered when measuring performance parameters, such as the working fluid's pressure amplitude and phase angle, needed for comparisons of predictions to test data.

Errors in predicting Stirling engine performance could be caused by unsatisfactory computer model precision, which relates to approximations made to simplify the solution of the governing conservation equations. These approximations included finite difference approximations to these equations and the decoupling of the momentum and energy equations in the NASA Lewis computer model. When considering these approximations, this study concluded that the treatment of these governing equations does not account for the inaccuracy seen in predicting engine performance.

Generally, the percentage error in predicting the GPU-3 power was larger than that for the P-40 or RE-1000 Stirling engines and, therefore, work went into understanding the pressure phase angle prediction error. The accuracy in predicting the GPU-3 pressure phase angle was found to be closely related to the accuracy in predicting the working fluid mass variation in the expansion space and compression space and the accuracy in predicting the gas temperature variation for the "hot-side" of the Stirling engine.

Modeling of the piston and displacer mass leakage past the seals could have an impact on the mass variation prediction; currently this effect is accounted for crudely or not at all (depending on the specific engine) in the Stirling engine computer code. Also, past work suggests that improvements to the hysteresis (cylinder heat transfer) model would alter the "hot-side" gas temperature variation prediction.

The cylinder hysteresis loss was increased for the GPU-3 and RE-1000 by increasing the heat transfer coefficients in the expansion and compression spaces. As a result, accuracy improved in power predictions for both engines because of decreases in the GPU-3 pressure phase angle error and the RE-1000 pressure amplitude error. Notice that an improvement was made in the prediction of the pressure parameter that was mainly responsible for the respective engine's power prediction error. This sensitivity study supports the suggestion that an improvement in the hysteresis loss model could significantly benefit Stirling engine performance predictions. One recommendation of this study is to improve the modeling of this hysteresis loss.

Much work remains to be done to understand the true physics of the Stirling engine. The different loss mechanisms need to be investigated in greater depth and their effort on engine performance understood. These loss mechanisms include: cylinder hysteresis loss, gas leakage loss, effect of oscillating flow on pressure drop and heat transfer, appendix gap loss, and velocity and temperature maldistributions. Currently, a significant "loss understanding" effort is being made in the area of oscillating flow effects. Also, studies are beginning on multidimensional analysis of the gas flow path.

APPENDIX A

ENGINE DIMENSIONS

Tables A.I, A.II, A.III, and A.IV give GPU-3, P-40, and RE-1000 Stirling engine dimensions and other operating parameters.

TABLE A.I - GPU-3 ENGINE DIMENSIONS AND PARAMETERS (FROM REF. 6)

Miscellaneous:	
Number of cylinders	1
Type of engine	Displacer
Type of drive	Rhombic
Type of shaft seals	Sliding
Cylinder bore with liner, cm (in.)	6.99 (2.75)
Cylinder bore above liner (top of displacer seal at top of liner at displacer top-dead-center), cm (in.)	7.01 (2.76)
Stroke, cm (in.)	3.15 (1.24)
Displacement (maximum change in total working-space volume), cm ³ (in. ³)	119.6 (7.30)
Piston-rod diameter, cm (in.)	2.22 (0.875)
Displacer-rod diameter, cm (in.)	0.953 (0.375)
Displacer diameter, cm (in.)	6.96 (2.74)
Displacer wall thickness, cm (in.)	0.159 (0.0625)
Expansion-space clearance, cm (in.)	0.163 (0.064)
Compression-space clearance, cm (in.)	0.030 (0.012)
Cooler:	
Tube length, cm (in.)	4.60 (1.81)
Heat-transfer length, cm (in.)	3.56 (1.40)
Tube inside diameter, cm (in.)	0.108 (0.0425)
Tube outside diameter, cm (in.)	0.159 (0.0625)
Number of tubes per cylinder	312
Number of tubes per cooler	39
Heater:	
Mean tube length, cm (in.)	
Regenerator side	12.90 (5.08)
Cylinder side	11.63 (4.58)
Heat-transfer length, cm (in.)	7.77 (3.06)
Tube inside diameter, cm (in.)	0.302 (0.119)
Tube outside diameter, cm (in.)	0.483 (0.190)
Number of tubes per cylinder (consider tubes to regenerator and cylinder separately)	80
Regenerators:	
Length (inside), cm (in.)	2.26 (0.89)
Diameter (inside), cm (in.)	2.26 (0.89)
Number per cylinder	8
Matrix:	
Wire-cloth material	304 stainless steel
Cloth mesh per 2.5 cm (1 in.)	200x200
Wire diameter, cm (in.)	0.00406 (0.0016)
Number of layers	308
Filler factor, percent	30.3
Drive:	
Connecting-rod length, cm (in.)	4.60 (1.81)
Crank radius, cm (in.)	1.38 (0.543)
Eccentricity, cm (in.)	2.08 (0.82)
Insulation covers:	
Cross-sectional area, cm ² (in. ²)	6.45 (1.00)
Length between thermocouples, cm (in.)	1.27 (0.50)

TABLE A.II - GPU-3 ENGINE DEAD VOLUMES (FROM REF. 6)

[All volumes in cm³ (in.³).]

Expansion space clearance volume:		
Clearance around displacer	3.34	(0.204)
Clearance above displacer	7.41	(0.452)
Volume from end of heater tubes into cylinder	<u>1.74</u>	<u>(0.106)</u>
Total	12.49	(0.762)
Heater dead volume:		
Insulated portion of tubes leading to expansion space	9.68	(0.591)
Heated portion fo tubes	47.46	(2.896)
Insulated portion of tubes leading to regenerator	13.29	(0.811)
Additional volume in four tubes used for instrumentation	2.74	(0.167)
Volume in header	<u>7.67</u>	<u>(0.468)</u>
Total	80.84	(4.933)
Regenerator dead volume:		
Volume between regenerators and heater tubes	8.75	(0.534)
Volume within matrix	50.60	(3.088)
Volume between regenerators and cooler tubes	<u>6.16</u>	<u>(0.376)</u>
Total	65.51	(3.998)
Cooler dead volume:		
Volume in cooler tubes	13.14	(0.802)
Compression-space clearance volume:		
Volume in connecting passages from cooler tubes to compression space	12.57	(0.767)
Clearance around power piston	7.36	(0.449)
Clearance between displacer and power piston	<u>1.26</u>	<u>(0.077)</u>
Total	21.19	(1.293)
Total dead volume	193.2	(11.79)
Minimum live volume (power piston at TDC)	<u>39.2</u>	<u>(2.39)</u>
Calculated minimum total working-space volume	232.4	(14.18)

TABLE A.III - P-40 ENGINE DIMENSIONS AND PARAMETERS

[All parameters pertain to one cylinder.]

Miscellaneous:		
Number of cylinders	4 (square 4 arrangement)	
Overall dimensions, cm (in.)	78.5x65.5x58.0 (30.9x25.8x22.8)	
Dry weight (including auxiliaries), kg (lbm)	329. (725.)	
Working gas	Hydrogen	
Drive	Dual crank, crankshafts geared to driveshaft	
Preheater type	Recuperative	
Piston rod seal type	Sliding (pumping Leningrader)	
Piston stroke, cm (in.)	4.000 (1.575)	
Piston diameter, cm (in.)	5.406 (2.128)	
Piston rod diameter, cm (in.)	1.200 (0.4724)	
Gap width between piston and cylinder, cm (in.)	0.0470 (0.01850)	
Piston height, cm (in.)	8.966 (3.530)	
Connecting rod length, cm (in.)	10.0 (3.937)	
Crank radius, cm (in.)	2.0 (0.7874)	
Heater:		
Heater type	Involute tabular	
Number of heater tubes	18	
Heater tube material	Multimet N-155	
Heater tube outside diameter, cm (in.)	0.450 (0.1772)	
Heater tube inside diameter, cm (in.)	0.30 (0.1181)	
Heater tube length, cm (in.)	28.07 (11.05)	
Effective heater tube length for heat transfer, cm (in.)	25.18 (9.913)	
Regenerators:		
Number of regenerators	2	
Regenerator material	304 stainless steel wire mesh gauze	
Regenerator matrix diameter, cm (in.)	5.70 (2.244)	
Regenerator matrix length, cm (in.)	3.90 (1.535)	
Regenerator matrix wire diameter, cm (in.)	0.0050 (0.001968)	
Regenerator matrix porosity	0.58	
Coolers:		
Number of coolers	2	
Number of cooler tubes per cooler	192	
Cooler tube outside diameter, cm (in.)	0.150 (0.05906)	
Cooler tube inside diameter, cm (in.)	0.10 (0.03937)	
Cooler tube length, cm (in.)	8.000 (3.150)	
Effective cooler tube length, cm (in.)	6.721 (2.646)	
Effective cooling water flow area through coolers, cm ² (in. ²)	20.10 (3.116)	
Connecting ducts:		
Average heater-tube manifold inside diameter, cm (in.)	0.50 (0.1968)	
Average expansion space/heater-tube manifold flow path length, cm (in.)	1.20 (0.4724)	
Average heater-tube/regenerator manifold flow path length, cm (in.)	1.30 (0.5118)	
Cooler/compression-space connecting duct diameter, cm (in.)	1.40 (0.5512)	
Cooler/compression-space connecting duct length, cm (in.)	8.40 (3.307)	
Cooler casing inside diameter, cm (in.)	4.80 (1.890)	
Engine dead volumes:		
Expansion-space clearance volume, cm ³ (in. ³)	1.810 (0.1104)	
Expansion-space/heater connecting duct volume, cm ³ (in. ³)	4.409 (0.2690)	
Heater dead volume, cm ³ (in. ³)	35.71 (2.179)	
Heater/regenerators connecting ducts volume, cm ³ (in. ³)	16.66 (1.016)	
Regenerators dead volume, cm ³ (in. ³)	115.5 (7.045)	
Regenerator/cooler connecting ducts volume, cm ³ (in. ³)	5.099 (0.3111)	
Coolers dead volume, cm ³ (in. ³)	24.13 (1.472)	
Coolers/compression-space connecting ducts volume, cm ³ (in. ³)	49.87 (3.043)	
Compression-space clearance volume, cm ³ (in. ³)	7.270 (0.4435)	
Hot appendix gap volume, cm ³ (in. ³)	7.220 (0.4405)	
Cold appendix gas volume, cm ³ (in. ³)	0.7220 (0.04405)	

TABLE A.IV - DESCRIPTION OF THE GEOMETRY OF THE RE-1000 (FROM REF. 8)

Miscellaneous:	
Number of cylinders	1
Housing weight, kg (lb)	416 (917)
Type	Free-piston with dashpot
Design working fluid	Helium
Design frequency, Hz	30
Design pressure, MPa	7.0
Bounce space volume, cm ³ (in. ³)	20,500 (1250)
Design power, W	1000
Design displacer phase angle, deg	45
Cylinder bore, cm (in.)	5.722 (2.2527)
Maximum displacer 1 stroke, cm (in.)	4.01 (1.579)
Displacer 1 length, cm (in.)	15.21 (5.99)
Maximum displacer 2 stroke, cm (in.)	5.18 (2.039)
Displacer 2 length, cm (in.)	14.05 (5.53)
Maximum power piston stroke, cm (in.)	4.35 (1.713)
Cooler:	
Description	135 rectangular gas passages
Passage width, cm (in.)	0.0508 (0.020)
Passage depth, cm (in.)	0.376 (0.148)
Length, cm (in.)	7.92 (3.118)
Flow area, cm ² (in. ²)	2.58 (0.400)
Wetted perimeter, cm (in.)	115.2 (45.354)
Volume, cm ³ (in. ³)	20.42 (1.246)
Heater:	
Description	Tabular
Tube material	Inconel 718
Number of tubes	34
Tube length, cm (in.)	18.34 (7.220)
Tube inside diameter, mm (in.)	2.362 (0.093)
Tube outside diameter, mm (in.)	3.175 (0.125)
Design maximum wall temperature, °C (°F)	650 (1202)
Regenerator:	
Length containing wire mesh, cm (in.)	6.446 (2.538)
Outside diameter, cm (in.)	7.18 (2.825)
Inside diameter, cm (in.)	6.07 (2.391)
Inner wall thickness, cm (in.)	0.13 (0.05)
Matrix material	304SS Metex
Wire diameter, mm (in.)	0.0889 (0.0035)
Porosity, regenerator 1, percent	75.9
Porosity, regenerator 2, percent	81.2
Weight of matrix, regenerator 1, g (lb)	139 (0.31)
Weight of matrix, regenerator 2, g (lb)	108 (0.24)
Pistons:	
Standard power piston oscillating mass, kg (lb)	5.97 (13.17)
Light power piston oscillating mass, kg (lb)	3.48 (7.67)
Power piston diameter, cm (in.)	5.718 (2.2514)
Displacer 1 mass, kg (lb)	0.426 (0.939)
Displacer 1 diameter, cm (in.)	5.67 (2.232)
Displacer 1 rod diameter, cm (in.)	1.663 (0.6548)
Displacer 1 bore, cm (in.)	1.666 (0.6560)
Displacer 2 mass, kg (lb)	0.381 (0.840)
Displacer 2 diameter, cm (in.)	5.67 (2.232)
Displacer 2 rod diameter, cm (in.)	1.806 (0.7110)
Displacer 2 bore, cm (in.)	1.808 (0.7118)

TABLE A.IV - Concluded.

Dead volumes:		
Displacer 1/cylinder annular gap, cm ³ (in. ³)	9.83	(0.60)
Displacer 2/cylinder annular gap, cm ³ (in. ³)	8.36	(0.51)
Expansion-space instrumentation ports, cm ³ (in. ³)	1.64	(0.10)
Expansion-space to heater tube junction, cm ³ (in. ³)	3.80	(0.23)
Heater tubes, cm ³ (in. ³)	27.4	(1.67)
Heater tube to regenerator plegum junction, cm ³ (in. ³)	5.90	(0.36)
Regenerator hot end plenum, cm ³ (in. ³)	4.10	(0.25)
Regenerator plenum ring, cm ³ (in. ³)	0.83	(0.05)
Instrumentation ports (heater/regenerator), cm ³ (in. ³)	1.64	(0.10)
Regenerator 1, cm ³ (in. ³)	56.1	(3.42)
Regenerator 2, cm ³ (in. ³)	69.1	(3.67)
Regenerator cold end plenum, cm ³ (in. ³)	4.23	(0.26)
Instrumentation ports (regenerator/cooler), cm ³ (in. ³)	3.41	(0.21)
Cooler, cm ³ (in. ³)	20.42	(1.25)
Cooler plenum at the compression space, cm ³ (in. ³)	7.15	(0.44)
Compression-space instrumentation ports, cm ³ (in. ³)	3.15	(0.19)
Cylinder ports, cm ³ (in. ³)	1.21	(0.07)
Piston/spider clearance, cm ³ (in. ³)	18.4	(1.21)
Annular ring around the spider, cm ³ (in. ³)	3.82	(0.23)
Displacer LVDT core, cm ³ (in. ³)	2.95	(0.18)
Power piston center port, cm ³ (in. ³)	5.90	(0.36)
Materials:		
Heater head		
Regenerator outer cylinder	316 stainless steel	
Expansion-space dome	316 stainless steel	
Regenerator inner cylinder wall	316 stainless steel	
Displacer	321 stainless steel	
Cooler	6061-T6 Al	
Cylinder		
Power piston	6016-T6 Al with chrome oxide coating	
Displacer	304 stainless steel with oxide coating	
Standard power piston	6061-T6 Al body with Xylan coating and mild steel mass	
Light power piston	6061-T6 Al body with Xylan coating and Al mass	
Diametral clearances:		
Displacer 1 rod/rod cylinder, mm (in.)	0.030	(0.0012)
Displacer 1 body/displacer cylinder, mm (in.)	0.381	(0.015)
Displacer 2 rod/rod cylinder, mm (in.)	0.020	(0.0008)
Displacer 2 body/displacer cylinder, mm (in.)	0.381	(0.015)
Power piston/piston cylinder, mm (in.)	0.033	(0.001)
Displacer gas spring:		
No. 1 design mean volume, cm ³ (in. ³)	31.79	(1.94)
No. 1 rod diameter, cm (in.)	1.663	(0.655)
No. 2 design mean volume, cm ³ (in. ³)	18.8	(1.147)
No. 2 rod diameter, cm (in.)	1.806	(0.711)
Center ports:		
Power piston port location (distance from inward limit to center port opening position), cm (in.)	2.05	(0.81)
Displacer 1 (distance from expansion space limit to position where the center port opens), cm (in.)	1.90	(0.75)
Displacer 2 (distance from expansion space limit to position where the center port opens), cm (in.)	2.64	(1.04)
Center port diameter (power piston), mm (in.)	1.1	(0.042)
Center port diameter (displacers), mm (in.)	1.0	(0.040)

APPENDIX B

ENGINE TEST DATA

Tables B.I, B.II, and B.III give the GPU-3, P-40, and RE-1000 Stirling engine test data used for this study computer code evaluation. All the engine test data were taken at NASA Lewis Research Center.

TABLE B.I -

Run identity	Mean pressure, MPa	Engine speed, rpm	Average heater-tube gas temperature, °C	Brake power, kW	Brake thermal efficiency, percent	Heat input, kW	Heat to cooler coolant, kW	Coolant ΔT across cooler, °C
Hydrogen								
H1-41B	2.86	3495	580	2.13	18.5	11.52	7.4	8.2
H1-43B	2.84	2499	584	2.04	24.4	8.39	5.3	5.9
H1-45B	2.85	1492	581	1.33	22.0	6.04	3.4	3.8
H3-41A	2.86	3519	681	2.71	24.2	11.23	7.3	8.3
H3-43A	2.85	2499	669	2.39	26.7	8.97	5.4	6.2
H3-45A	2.86	1471	679	1.50	24.3	6.19	3.6	4.1
H3-61A	4.23	3516	687	4.47	28.3	15.79	10.5	11.5
H25-64B	4.25	2002	652	2.93	29.1	10.07	6.0	6.6
H25-65B	4.25	1501	659	2.30	30.8	7.48	4.7	5.2
H25-104A	6.98	1999	663	5.24	33.3	15.72	9.2	9.8
H25-105A	7.02	1504	659	4.16	34.5	12.08	7.1	7.6
Helium								
HE1-41A	2.86	3516	593	0.26	2.7	9.59	8.1	9.1
H31-43A	2.84	2506	580	0.94	12.8	7.34	5.6	6.3
HE1-45A	2.84	1501	574	0.92	17.6	5.24	3.5	4.0
HE3-41B	2.90	3494	698	0.95	8.8	10.81	8.3	9.0
HE3-43B	2.86	2520	701	1.53	19.0	8.07	5.9	6.4
HE3-45A	2.86	1515	701	1.25	10.0	6.24	3.8	4.1
HE3-61A	4.28	3499	683	2.03	12.6	16.17	11.4	13.5
HE3-62A	4.23	3009	698	2.58	18.3	14.11	9.9	11.9
HE3-64B	4.20	1995	706	2.40	23.4	10.26	6.5	8.4
HE3-81A	5.61	3512	685	3.42	18.1	18.92	14.4	18.5
HE3-82A	5.63	3019	690	3.77	20.8	18.09	12.4	16.3

^aAmplitude - peak-to-peak values.

^bPhase angle - angle between the maximum gas pressure and minimum expansion-space volume.

TABLE B.II -

Run identity	Mean pressure, MPa	Engine speed, rpm	Brake power, kW	Brake thermal efficiency, percent	Heat input, kW	Heat to cooler coolant, kW	Coolant ΔT across cooler, °C
388	5.12	947	4.78	28.3	16.9	11.3	2.0
395	5.11	2000	9.47	32.0	29.6	19.0	2.3
396	5.13	3002	13.11	32.7	40.1	25.6	2.1
387	5.10	3918	15.02	28.7	52.4	35.1	2.5
393	10.12	997	9.95	33.6	29.7	18.9	3.6
397	10.08	2000	19.18	35.7	53.7	33.4	4.0
386	10.13	3003	26.14	33.4	78.3	50.5	4.3
394	10.15	4001	31.29	31.9	98.0	64.4	4.5
389	15.13	1413	21.70	36.9	58.8	36.2	5.7
391	15.08	2002	27.79	36.4	76.4	47.3	5.6
392	15.09	2999	37.48	34.3	109.3	69.8	5.7
390	15.17	4000	43.21	30.3	142.5	96.7	6.7

^aAmplitude - peak-to-peak values.

GPU-3 TEST DATA

Expansion-space heater duct gas temperature, °C	Cooler-compression-space duct gas temperature, °C	Expansion-space pressure amplitude, ^a MPa	Compression-space pressure amplitude, ^a MPa	Expansion-space pressure phase angle, ^b deg	Compression-space pressure phase angle, ^b deg	Energy balance error, percent
working fluid						
557	72	1.84	1.78	300	300	6.2
569	61	1.76	1.82	300	300	2.5
553	52	1.74	1.80	300	300	8.1
643	70	1.84	1.82	300	300	1.3
617	62	1.82	1.82	300	300	2.5
634	53	1.72	1.84	300	300	5.0
660	86	2.73	2.63	300	300	-1.3
638	68	2.54	2.70	304	300	2.8
623	63	2.49	2.70	306	303	-1.5
655	80	4.22	4.42	300	300	1.4
637	72	4.23	4.43	303	304	0.6
working fluid						
572	98	1.74	1.96	300	300	0.4
548	82	1.69	1.90	300	295	-1.0
551	66	1.80	1.88	300	300	1.8
677	95	1.82	2.00	300	300	1.9
668	80	1.86	1.94	300	300	-1.6
674	70	1.88	1.76	305	305	5.3
677	117	2.77	2.46	300	300	4.8
677	106	2.77	2.87	300	300	1.0
672	87	2.81	2.85	300	300	2.5
671	123	3.53	3.66	300	300	-1.6
674	113	3.64	3.68	300	300	1.5

P-40 TEST DATA

Expansion-space heater duct gas temperature, °C	Cooler-compression-space duct gas temperature, °C	Maximum compression-space pressure, MPa	Minimum compression-space pressure, MPa	Compression-space pressure ratio	Compression-space pressure amplitude, ^a MPa
657	57	6.27	3.89	1.60	2.38
659	57	6.26	3.86	1.61	2.41
654	57	6.30	3.85	1.62	2.44
646	59	6.30	3.83	1.63	2.47
660	59	12.53	7.73	1.61	4.81
639	60	12.50	7.69	1.62	4.82
628	62	12.57	7.71	1.62	4.87
613	63	12.49	7.68	1.62	4.81
640	62	18.86	11.55	1.63	7.32
623	63	18.79	11.50	1.63	7.29
597	65	18.65	11.45	1.62	7.19
575	69	18.73	11.51	1.62	7.22

TABLE B.III - RE-1000

Run identity	Mean pressure, MPa	Piston stroke, cm	Average heater wall temperature, °C	Cooling water inlet temperature, °C	Engine frequency, Hz	Indicated power, W	Indicated efficiency, percent	Heat input, W	Heat to cooler coolant, W	Expansion-space gas temperature, °C
1006	7.04	1.80	600	25	30.2	570	24.4	2338	1892	568
1010	7.03	2.60	599	25	30.1	939	25.8	3643	2736	558
1012	7.05	3.00	599	25	30.2	1100	24.6	4467	3265	552
1017	7.06	2.60	550	25	30.2	846	24.7	3424	2713	511
1024	7.05	2.60	500	25	30.2	765	22.8	3348	2681	462
1030	7.06	2.60	450	25	30.2	643	20.4	3159	2595	415
1070	5.53	2.61	599	25	26.9	759	26.4	2879	2137	555
1079	4.01	2.61	599	25	23.0	520	24.7	2109	1242	553
1121	7.07	2.61	600	40	30.3	907	25.2	3599	2532	557
1200	7.03	2.60	600	55	30.2	837	24.0	3493	2108	558

^aAmplitude - peak-to-peak values.

^bPhase angle - angle between the maximum gas pressure and minimum working space volume.

^cP - gas pressure.

TEST DATA

Regenerator-heater gas temperature, °C	Regenerator-cooler gas temperature, °C	Compression-space gas temperature, °C	Compression-space pressure amplitude, ^a kPa	Compression-space pressure phase angle, ^b deg	Cooler WP, ^c kPa	Regenerator WP, ^c kPa	Displacer WP, ^c kPa
564	91	40	792	-19.8	3	40	70
548	91	56	1147	-15.7	7	60	100
540	93	65	1344	-14.0	10	60	100
507	92	53	1166	-14.1	7	60	100
461	90	54	1176	-12.5	7	60	100
416	89	55	1181	-10.3	7	60	100
555	80	49	910	-18.0	4	40	70
560	70	42	645	-19.7	3	30	50
559	109	64	1171	-14.9	6	60	100
559	123	75	1161	-13.7	6	50	90

APPENDIX C

DESCRIPTION OF THE PWCF CODE

The Pressure-Wave Curve-Fit (PWCF) computer code was used to calculate the Stirling engine power given mean gas pressures, pressure amplitudes, and pressure phase angles for both the expansion space and compression space.

The gas pressure parameters were curve-fit in the following manner:

$$P_e = P_{em} + \frac{1}{2} P_{ea} \sin[\alpha + \beta_e(\alpha)]$$

$$P_c = P_{cm} + \frac{1}{2} P_{ca} \sin[\alpha + \beta_c(\alpha)]$$

where P_{em} is the mean expansion-space gas pressure, P_{ea} is the expansion-space gas pressure amplitude (defined as maximum pressure - minimum pressure), α is the engine crank angle or piston angular position, β_e is the expansion-space pressure phase angle, β varies linearly with α in order to simulate the nonharmonic nature of the Stirling engine gas pressure variation with time, and the subscript c indicates compression-space gas pressure parameters.

Having a mathematical relationship for the Stirling engine gas pressure, it was straightforward to calculate the Stirling engine indicated power and heat input. Work per cycle is $\oint (P_e dV_e + P_c dV_c)$. Heat input was approximated as $\oint (P_e dV_e)$. The integration was accomplished numerically and both expressions were multiplied by engine frequency to arrive at power or energy flow rate.

The accuracy of the PWCF code was evaluated by comparing the PWCF code's calculated value of Stirling engine indicated power to that predicted from the NASA Stirling engine computer simulation. Indicated power errors resulting from the use of this PWCF code at design conditions are

GPU-3 error = 1 percent

P-40 error = 8 percent

RE-1000 error = 1 percent

Thus, the PWCF code was considered sufficiently accurate for calculating indicated power.

Heat input calculated with the PWCF code was compared to that predicted from the NASA Stirling engine computer simulation. The discrepancy was 40 to 50 percent for all three engines, and thus this PWCF code was not considered accurate enough for calculating heat input.

REFERENCES

1. Tew, R.C., Jr.: Computer Program for Stirling Engine Performance Calculations. NASA TM-82960, DOE/NASA/51040-42, 1983.
2. Tew, R.C., Jr.; Thieme, L.G.; and Miao, D.: Initial Comparison of Single Cylinder Stirling Engine Computer Model Predictions With Test Results. NASA TM-79044, DOE/NASA/1040-78/30, 1979.
3. Allen, D.; and Cairelli, J.: Test Results of a 40kW Stirling Engine and Comparison With the NASA-Lewis Computer Code Predictions. Energy For the Twenty-First Century (20th IECEC), Vol. 3, SAE, 1985, pp. 3.238-3.243. (NASA TM-87050.)
4. Tew, R.C., Jr.: Comparison of Free-Piston Stirling Engine Model Predictions with RE-1000 Engine Test Data. NASA TM-83650, DOE/NASA/1005-3, 1984.
5. Geng, S.M.: Calibration and Comparison of the NASA Lewis Free-Piston Stirling Engine Model Predictions with RE-1000 Test Data. NASA TM-89853, 1987.
6. Thieme, L.G.: Low-Power Baseline Test Results for the GPU-3 Stirling Engine. NASA TM-79103, DOE/NASA/1040-79/6, 1979.
7. Kelm, G.G.; Cairelli, J.E.; and Walter, R.J.: Test Results and Facility Description for a 40-Kilowatt Stirling Engine. NASA TM-82620, DOE/NASA/51040-27, 1981.
8. Schreiber, J.G.: Testing and Performance Characteristics of a 1-kW Free-Piston Stirling Engine. NASA TM-82999, 1983.
9. Giansante, J.E.: A Free Piston Stirling Engine Performance Code. Report 81TR17, Mechanical Technology, Inc., Latham, NY, Nov. 1980.
10. Sullivan, T.J.: Comparison of NASA Lewis Performance Code's Pressure-Drop Model Predictions to Stirling Engine Working-Space Flow Test Data. NASA CR-182215, 1988.
11. Thieme, L.G.: High-Power Baseline and Motoring Test Results for the GPU-3 Stirling Engine. NASA TM-82646, DOE/NASA/51040-31, 1981.
12. Schreiber, J.G.; Geng, S.M.; and Lorenz, G.V.: RE-1000 Free-Piston Stirling Engine Sensitivity Test Results. NASA TM-88846, DOE/NASA/1005-11, 1986.
13. Faulkner, H.B.; and Smith, J.L., Jr.: Instantaneous Heat Transfer During Compression and Expansion in Reciprocating Gas Handling Machinery. Energy for the Marketplace (18th IECEC), Vol. 2, AIChE, 1983, pp. 724-730.

TABLE I. - STIRLING ENGINE DESIGN OPERATING CONDITIONS

GPU-3	
Gas mean pressure, MPa	6.9
Engine speed, rpm	3000
Average heater gas temperature, °C	677
Coolant inlet temperature, °C	20
Coolant	Water
Working fluid	H ₂
P-40	
Gas mean pressure, MPa	15.0
Engine speed, rpm	4000
Average heater wall temperature, °C	720
Coolant inlet temperature, °C	50
Coolant	Water
Working fluid	H ₂
RE-1000	
Gas mean pressure, MPa	7.0
Piston stroke, cm	2.6
Average heater wall temperature, °C	600
Engine frequency, Hz	30
Coolant inlet temperature, °C	25
Coolant	Water
Working fluid	He

TABLE II. - STIRLING ENGINE COMPUTER MODEL INPUTS

Engine geometry

Code space and time specifications:

- Number of engine cycles
- Number of control volumes for each component
- Number of time steps per cycle

Code options:

- Working fluid - real, ideal (real used for this study)
- Gas type - H₂, He, mixture
- Heater temperature - wall, gas
- RE-1000 - input piston motion or solve for piston motion (input used for this study)

Engine operating conditions:

- Mean gas pressure
- Engine speed
- Heater wall or average gas temperature
- Cylinder wall and regenerator wall temperatures
- Coolant flow rate
- Coolant inlet temperature

TABLE III. - STIRLING

Operating conditions (a)	Power, ^b percent	Efficiency, percent	Heat input, percent	Heat to coolant, percent
GPU-3 (H ₂)				
P = 2.8 MPa, W = 2500 rpm	38.0	14.8	20.1	23.4
P = 6.9 MPa, W = 2000 rpm (near design)	16.0	-1.6	17.9	21.6
GPU-3 (He)				
P = 2.8 MPa, W = 2500 rpm	129.1	78.2	28.6	14.9
P = 5.5 MPa, W = 3500 rpm	80.1	45.1	24.1	9.5
P-40 (H ₂)				
P = 5 MPa, W = 1000 rpm	-8.8	-14.6	6.8	7.5
P = 15 MPa, W = 4000 rpm (design)	-11.4	-3.9	-7.8	-17.3
RE-1000 (He)				
P = 4 MPa, St = 2.6 cm	20.1	8.9	10.3	27.5
P = 7 MPa, St = 1.8 cm	1.5	-4.1	5.8	-5.4
P = 7 MPa, St = 2.6 cm (design)	12.4	-8	13.0	5.4

^ap = mean pressure, W = engine speed, and St = piston stroke.

^bBrake values for the GPU-3 and P-40; indicated values for the RE-1000.

ENGINE PREDICTION ERRORS

Expansion-space gas temperature, °C	Compression-space gas temperature, °C	Expansion-space pressure amplitude, percent	Compression-space pressure amplitude, percent	Compression-space pressure phase angle, deg	Heat exchanger pressure drop amplitude, percent
working fluid)					
-1 -7	7 12	7.4 12.8	7.7 9.0	~6 ~6	--- ---
working fluid)					
5 -11	4 7	17.8 10.8	12.1 15.8	~7 ~5	--- ---
working fluid)					
30 11	5 24	--- 9.0	4.0 2.7	--- ---	--- ---
working fluid)					
2 4 -1	2 5 6	--- --- ---	11.3 5.4 7.1	1.4 -1.3 -0.1	-49 -51 -47

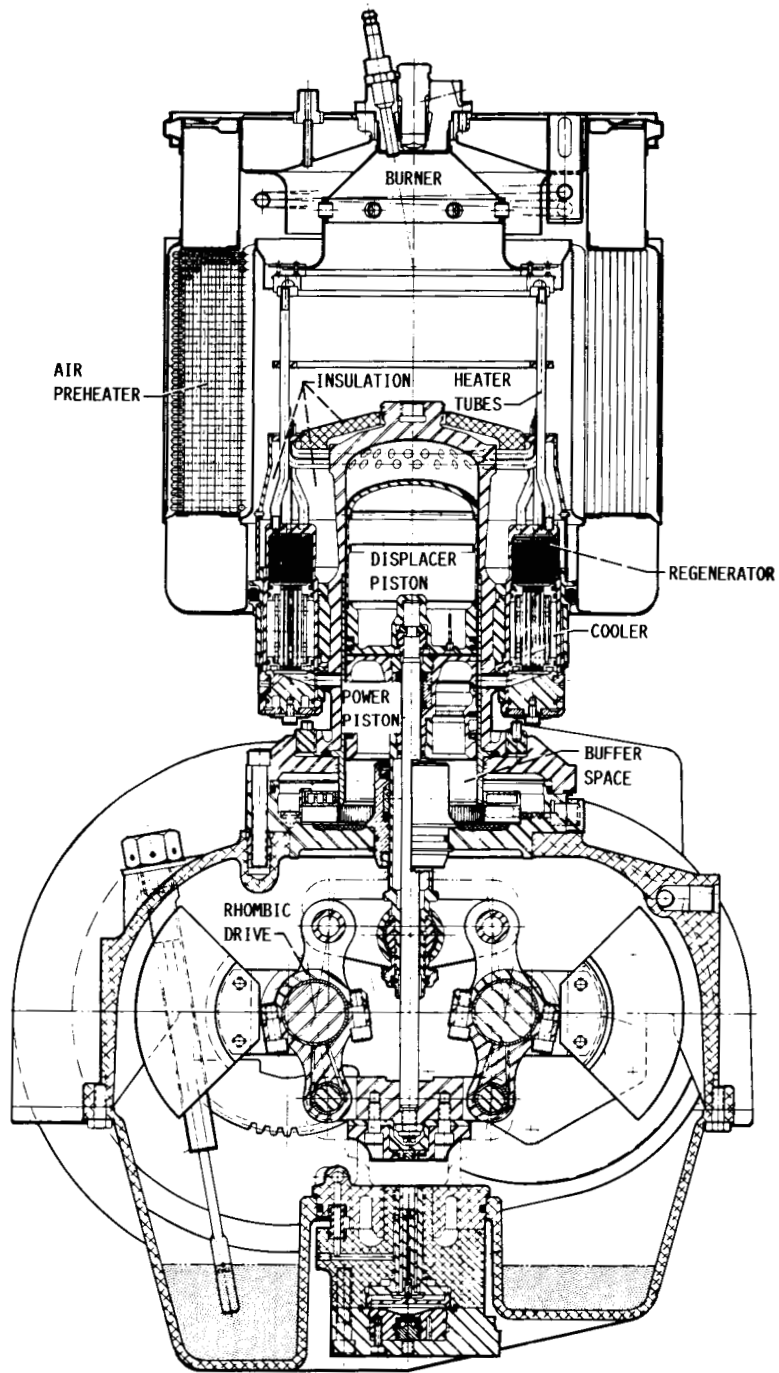


FIGURE 1. - CROSS-SECTIONAL VIEW OF GPU-3 SINGLE-CYLINDER STIRLING ENGINE.
 THE HYDROGEN COMPRESSOR WAS REMOVED FROM THE NASA TEST ENGINE.

ORIGINAL PAGE
 BLACK AND WHITE PHOTOGRAPH

ORIGINAL PAGE
BLACK AND WHITE PHOTOGRAPH

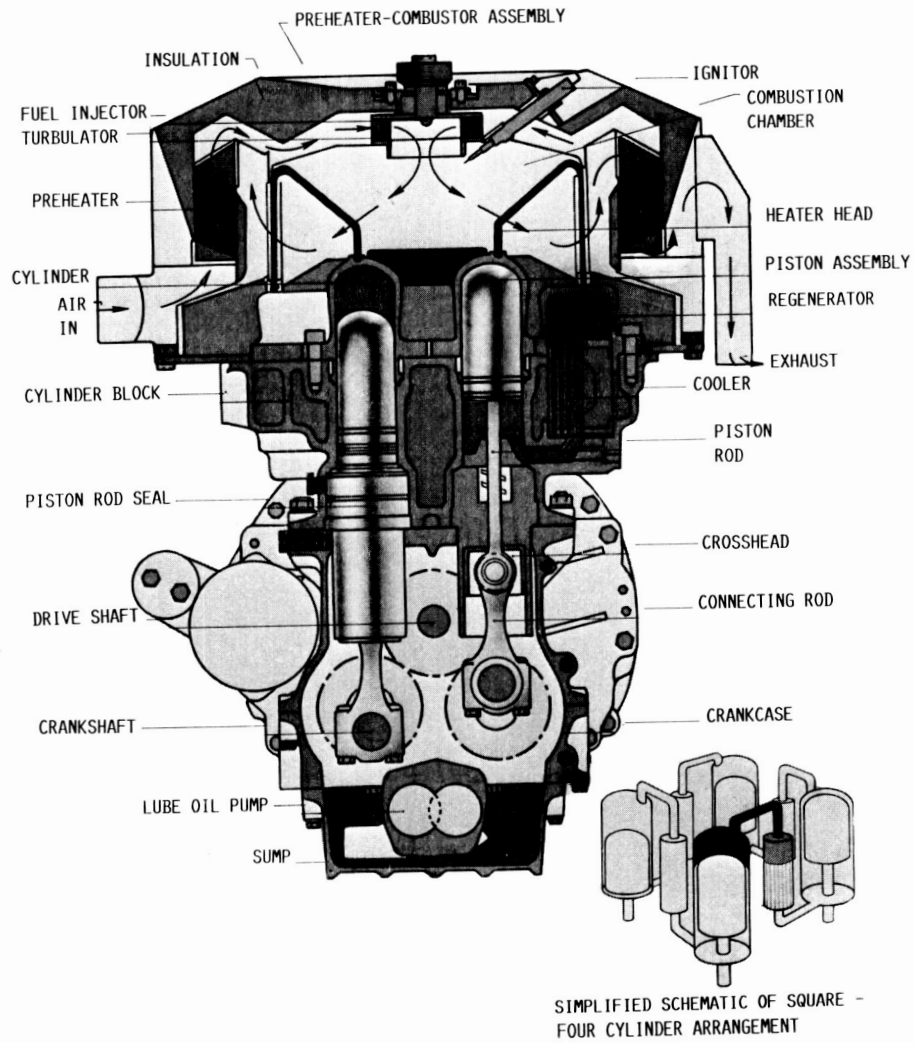


FIGURE 2. - CROSS-SECTIONAL VIEW OF P-40 STIRLING ENGINE.

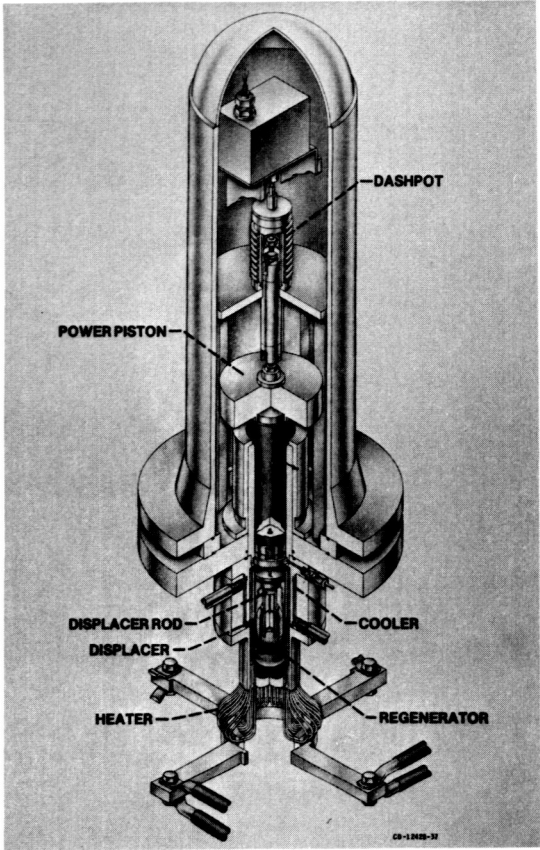


FIGURE 3. - CROSS-SECTIONAL VIEW OF RE-1000 FREE-PISTON STIRLING ENGINE.

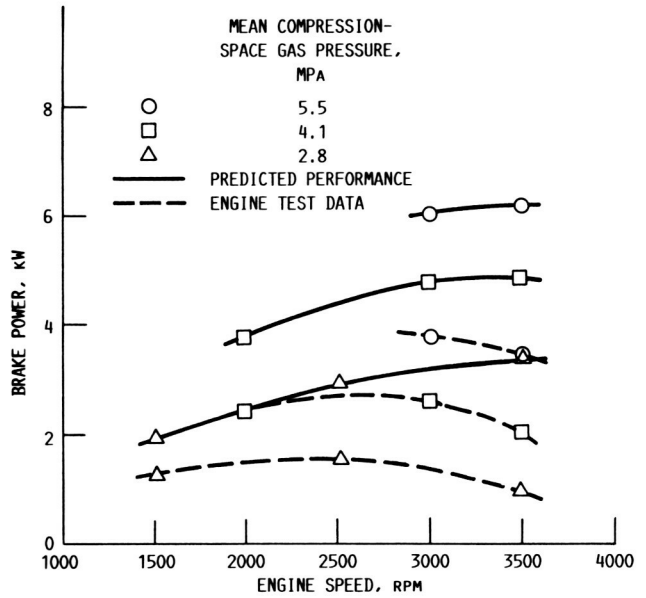


FIGURE 5. - GPU-3 BRAKE POWER VERSUS ENGINE SPEED FOR VARIOUS MEAN COMPRESSION-SPACE PRESSURES. AVERAGE HEATER-TUBE GAS TEMPERATURE, 690 °C; WORKING GAS, HELIUM.

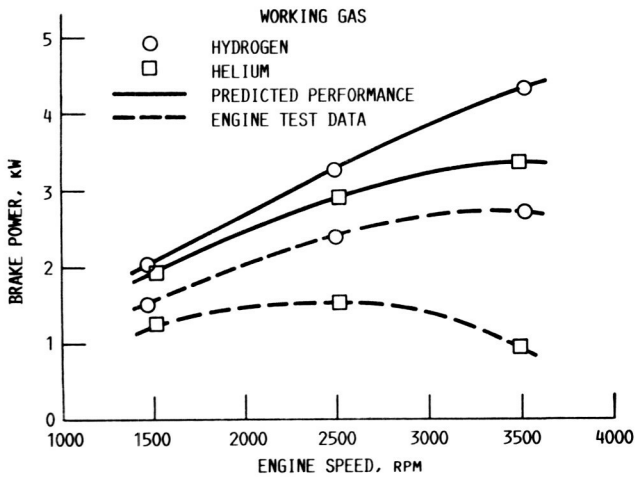


FIGURE 4. - GPU-3 BRAKE POWER VERSUS ENGINE SPEED FOR HYDROGEN AND HELIUM WORKING FLUIDS. AVERAGE HEATER-TUBE GAS TEMPERATURE, 690 °C; MEAN COMPRESSION-SPACE GAS PRESSURE, 2.8 MPa.

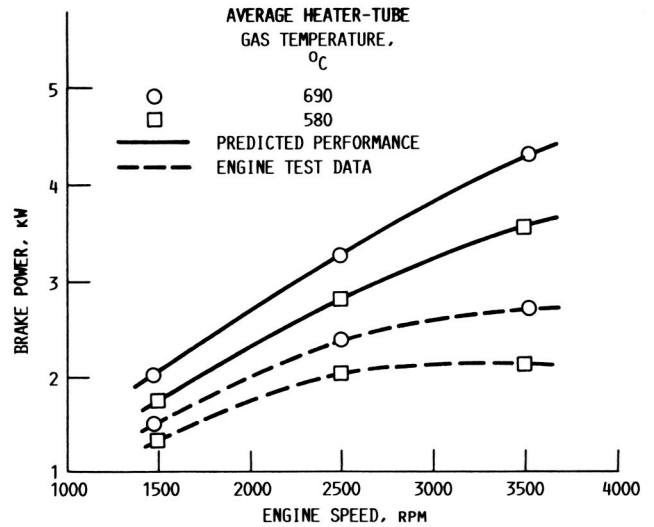


FIGURE 6. - GPU-3 BRAKE POWER VERSUS ENGINE SPEED FOR VARIOUS HEATER-TUBE GAS TEMPERATURES. MEAN COMPRESSION-SPACE PRESSURE, 2.8 MPa; WORKING GAS, HYDROGEN.

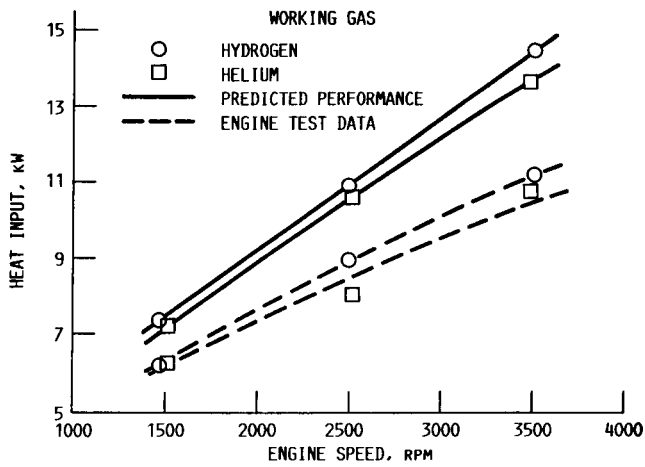


FIGURE 7. - GPU-3 HEAT INPUT VERSUS ENGINE SPEED FOR HYDROGEN AND HELIUM WORKING FLUIDS. AVERAGE HEATER-TUBE GAS TEMPERATURE, 690 °C; MEAN GAS PRESSURE, 2.8 MPa.

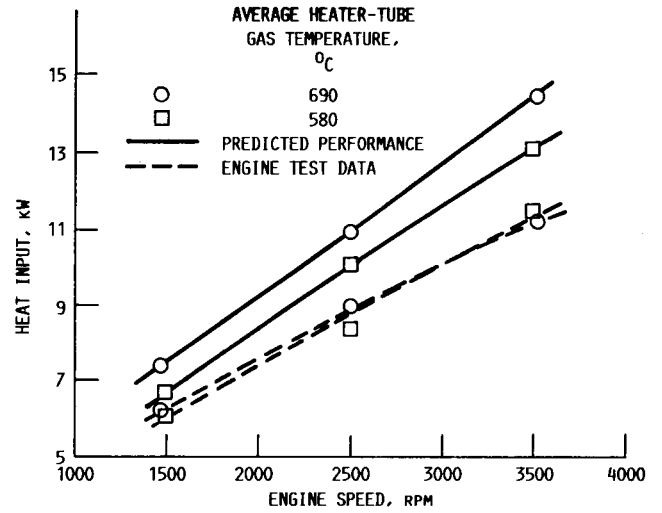


FIGURE 9. - GPU-3 HEAT INPUT VERSUS ENGINE SPEED FOR VARIOUS HEATER-TUBE GAS TEMPERATURES. MEAN COMPRESSION-SPACE PRESSURE IS 2.8 MPa, WORKING GAS, HYDROGEN.

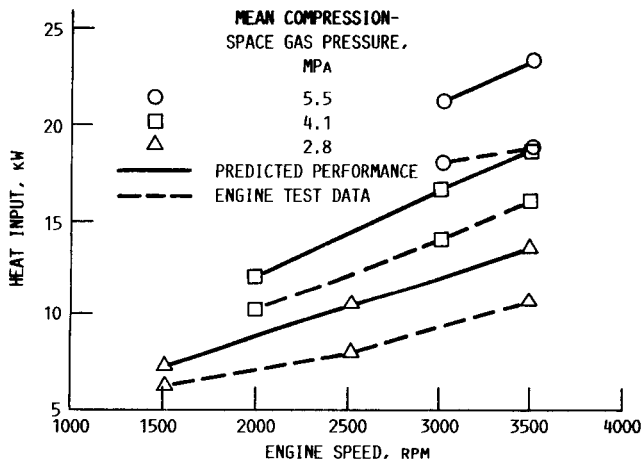


FIGURE 8. - GPU-3 HEAT INPUT VERSUS ENGINE SPEED FOR VARIOUS MEAN COMPRESSION-SPACE PRESSURES. AVERAGE HEATER-TUBE GAS TEMPERATURE, 690 °C; WORKING GAS, HELIUM.

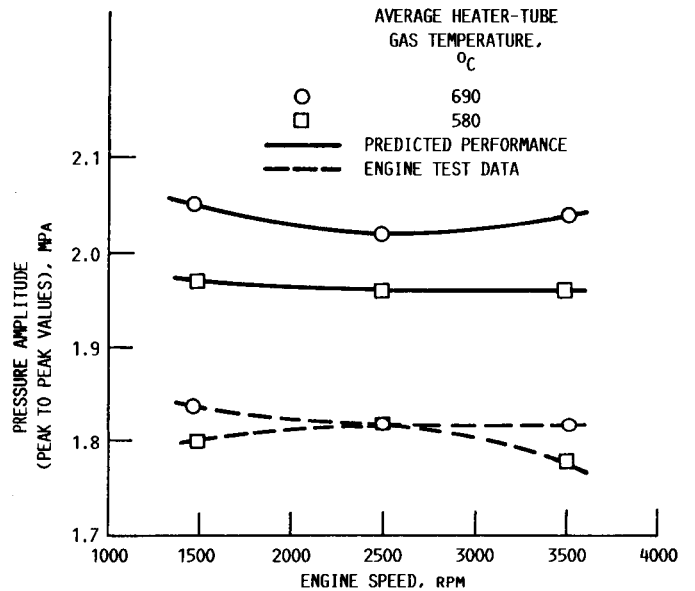


FIGURE 10. - GPU-3 COMPRESSION-SPACE PRESSURE AMPLITUDE (PEAK TO PEAK VALUES) VERSUS ENGINE SPEED FOR VARIOUS HEATER-TUBE GAS TEMPERATURES. MEAN COMPRESSION-SPACE PRESSURE, 2.8 MPa; WORKING GAS, HYDROGEN.

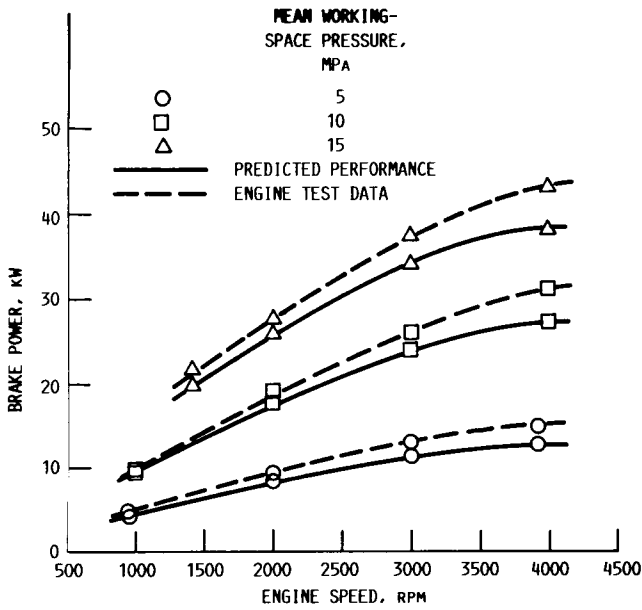


FIGURE 11. - P-40 BRAKE POWER VERSUS ENGINE SPEED FOR VARIOUS MEAN WORKING-SPACE PRESSURES. MEAN HEATER WALL TEMPERATURE, 720 °C.

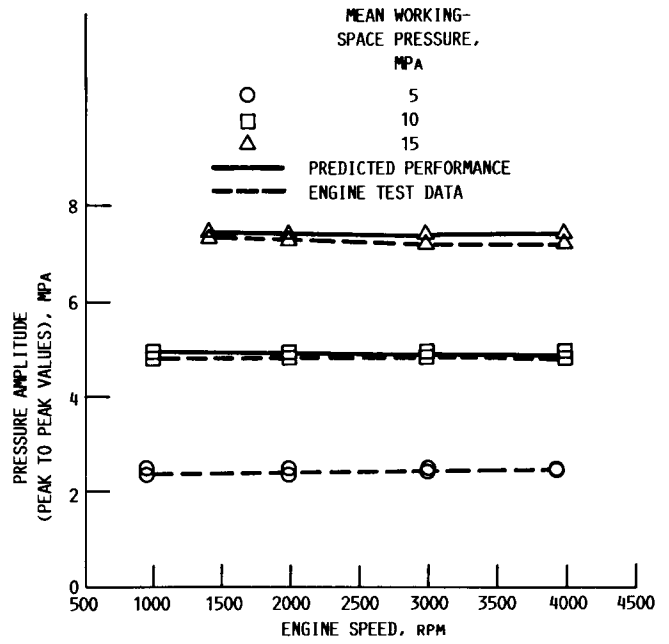


FIGURE 13. - P-40 COMPRESSION-SPACE PRESSURE AMPLITUDE (PEAK TO PEAK VALUES) VERSUS ENGINE SPEED FOR VARIOUS MEAN WORKING-SPACE PRESSURES. MEAN HEATER WALL TEMPERATURE, 720 °C.

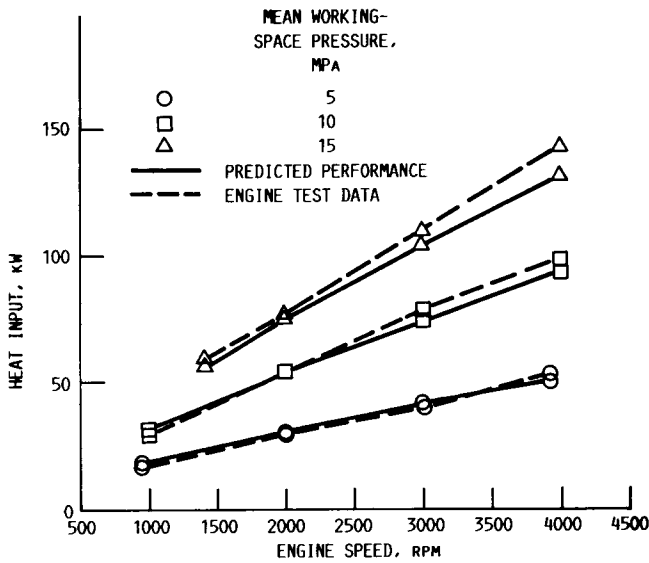


FIGURE 12. - P-40 HEAT INPUT VERSUS ENGINE SPEED FOR VARIOUS MEAN WORKING-SPACE PRESSURES. MEAN HEATER WALL TEMPERATURE, 720 °C.

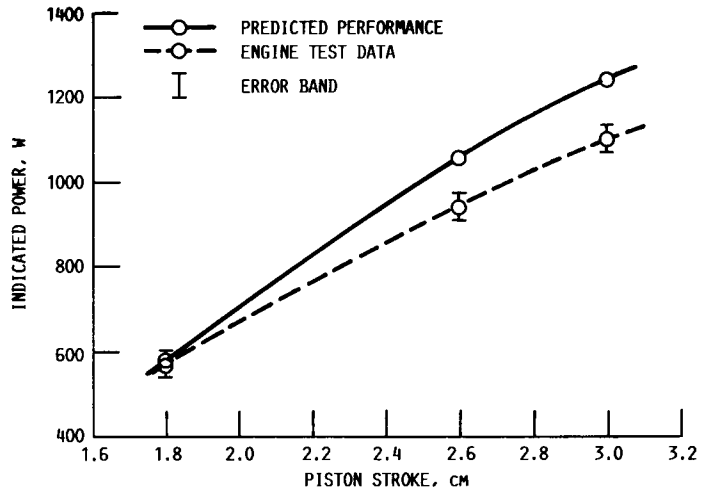


FIGURE 14. - RE-1000 INDICATED POWER VERSUS PISTON STROKE. MEAN WORKING-SPACE PRESSURE, 7.0 MPa; MEAN HEATER WALL TEMPERATURE, 600 °C; COOLANT INLET TEMPERATURE, 25 °C.

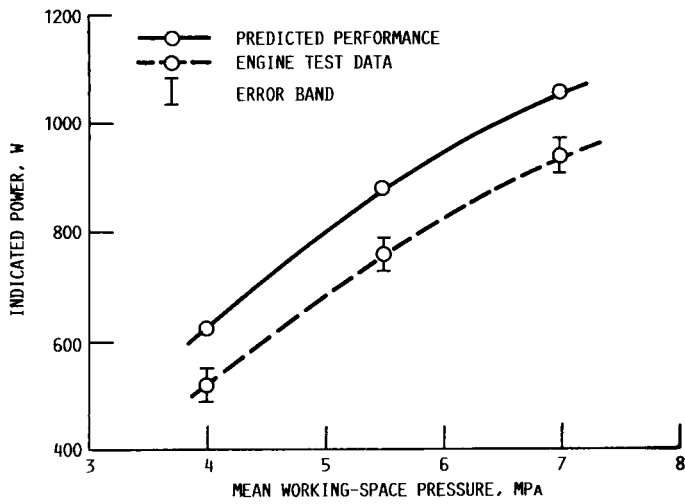


FIGURE 15. - RE-1000 INDICATED POWER VERSUS MEAN WORKING-SPACE PRESSURE. PISTON STROKE, 2.6 CM; MEAN HEATER WALL TEMPERATURE, 600 °C; COOLANT INLET TEMPERATURE, 25 °C.

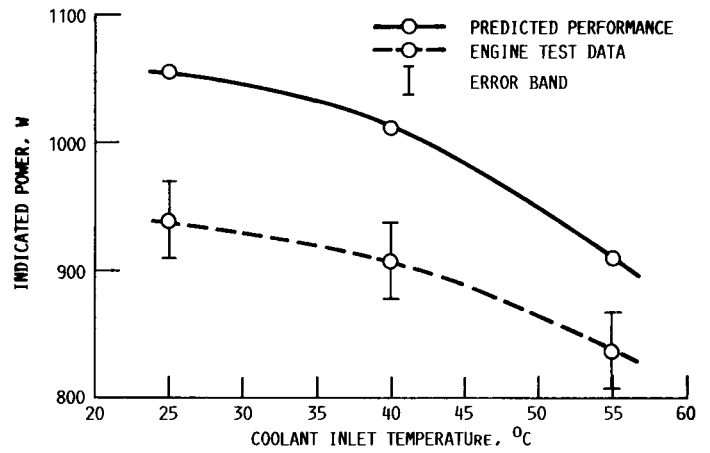


FIGURE 17. - RE-1000 INDICATED POWER VERSUS COOLANT INLET TEMPERATURE. PISTON STROKE, 2.6 CM; MEAN WORKING-SPACE PRESSURE, 7.0 MPa; MEAN HEATER WALL TEMPERATURE, 600 °C.

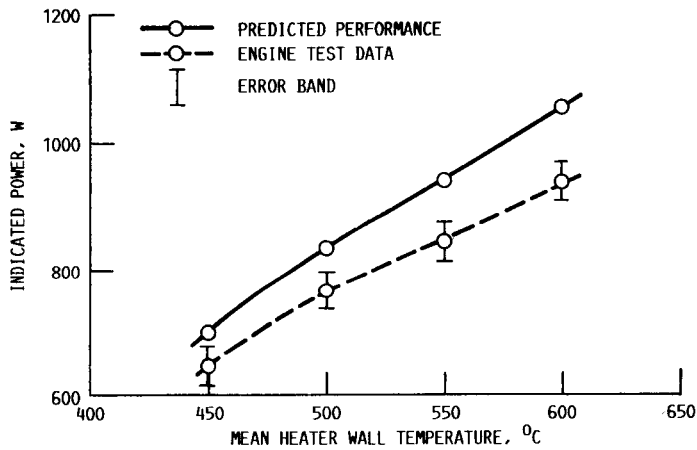


FIGURE 16. - RE-1000 INDICATED POWER VERSUS MEAN HEATER WALL TEMPERATURE. PISTON STROKE, 2.6 CM; MEAN WORKING-SPACE PRESSURE, 7.0 MPa; COOLANT INLET TEMPERATURE, 25 °C.

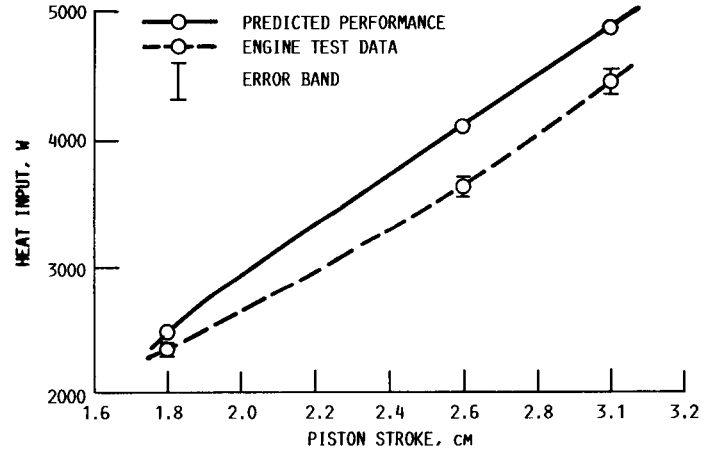


FIGURE 18. - RE-1000 HEAT INPUT VERSUS PISTON STROKE. MEAN WORKING-SPACE PRESSURE, 7.0 MPa; MEAN HEATER WALL TEMPERATURE, 600 °C; COOLANT INLET TEMPERATURE, 25 °C.

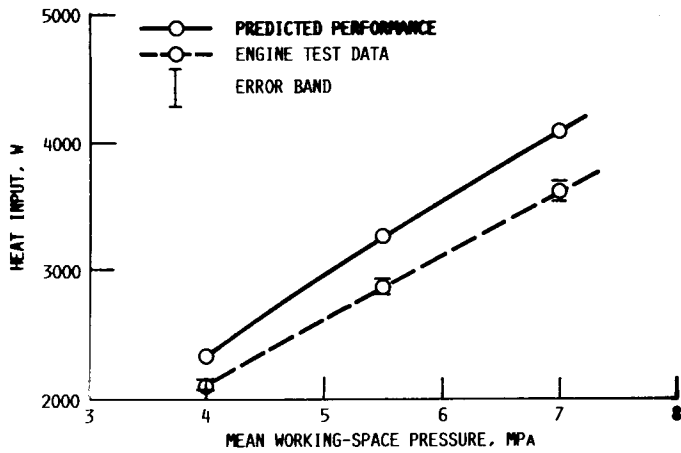


FIGURE 19. - RE-1000 HEAT INPUT VERSUS MEAN WORKING-SPACE PRESSURE. PISTON STROKE, 2.6 CM; MEAN HEATER WALL TEMPERATURE, 600 °C; COOLANT INLET TEMPERATURE, 25 °C.

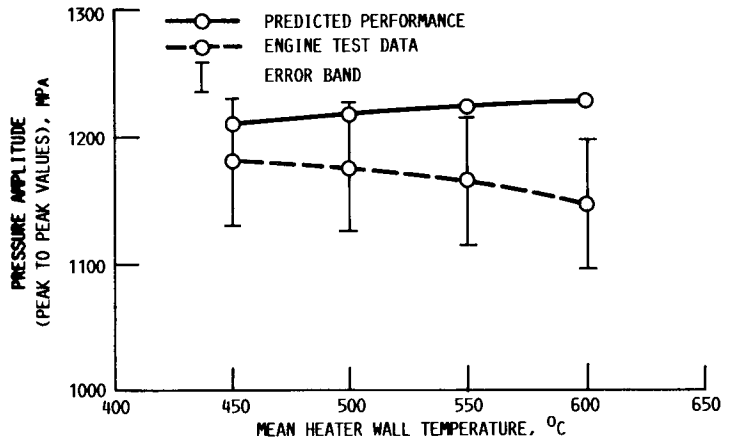


FIGURE 22. - RE-1000 COMPRESSION-SPACE PRESSURE AMPLITUDE (PEAK TO PEAK VALUES) VERSUS MEAN HEATER WALL TEMPERATURE. PISTON STROKE, 2.6 CM; MEAN WORKING-SPACE PRESSURE, 7.0 MPa; COOLANT INLET TEMPERATURE, 25 °C.

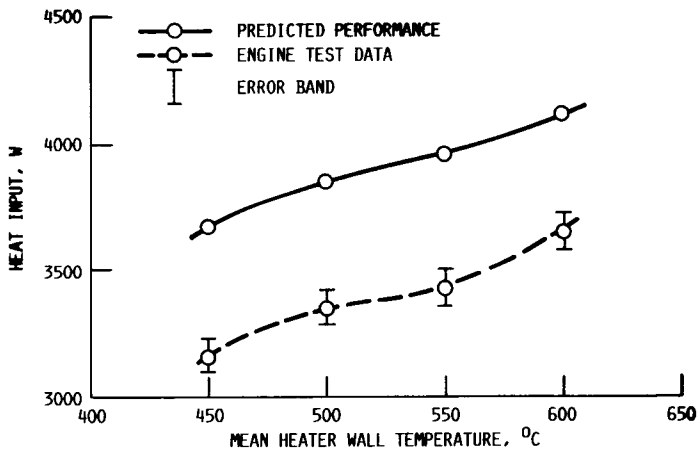


FIGURE 20. - RE-1000 HEAT INPUT VERSUS MEAN HEATER WALL TEMPERATURE. PISTON STROKE, 2.6 CM; MEAN WORKING-SPACE PRESSURE, 7.0 MPa; COOLANT INLET TEMPERATURE, 25 °C.

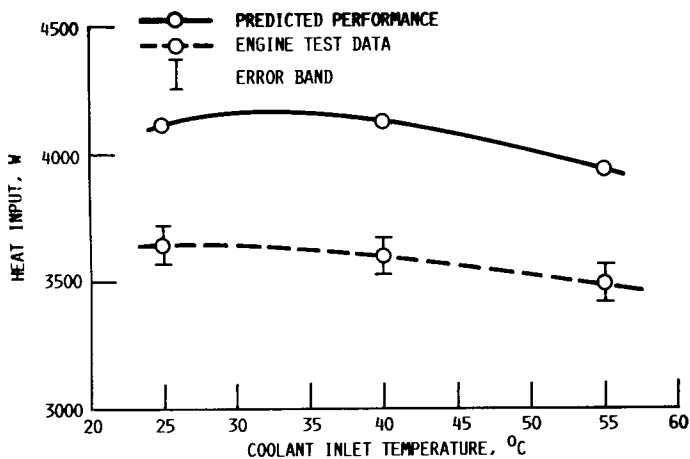


FIGURE 21. - RE-1000 HEAT INPUT VERSUS COOLANT INLET TEMPERATURE. PISTON STROKE, 2.6 CM; MEAN WORKING-SPACE PRESSURE, 7.0 MPa; MEAN HEATER WALL TEMPERATURE, 600 °C.

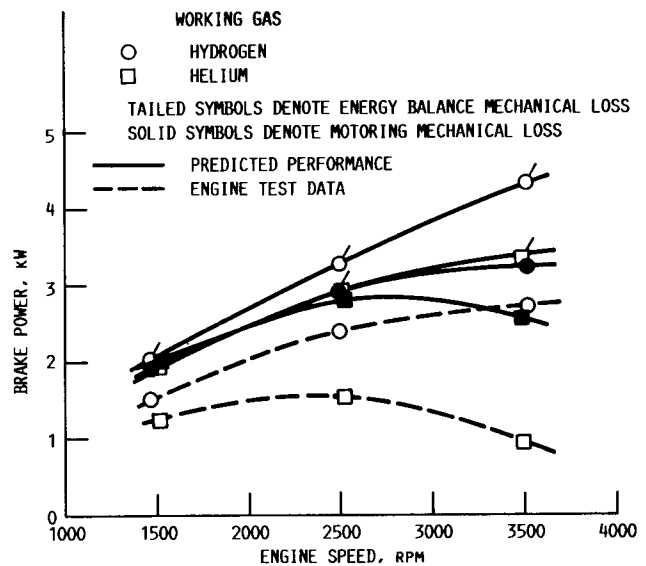


FIGURE 23. - GPU-3 BRAKE POWER VERSUS ENGINE SPEED, FOR DIFFERENT PREDICTIONS OF THE MECHANICAL LOSS. AVERAGE HEATER-TUBE GAS TEMPERATURE, 690 °C; MEAN COMPRESSION-SPACE PRESSURE, 2.8 MPa.

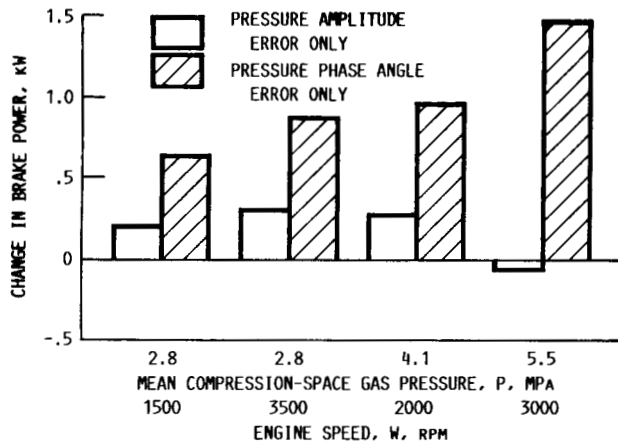


FIGURE 24. - GPU-3 BRAKE POWER SENSITIVITY DUE TO PREDICTION ERRORS IN THE PRESSURE AMPLITUDE OR PHASE ANGLE. WORKING GAS, HELIUM.

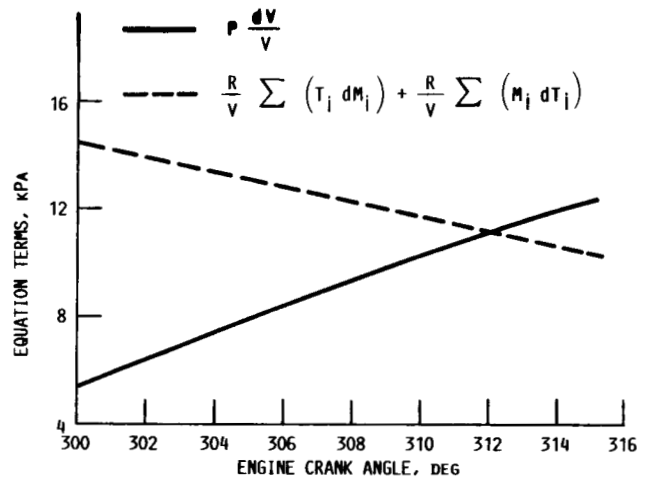


FIGURE 26. - GPU-3 PHASE ANGLE GOVERNING EQUATION CURVES. ENGINE SPEED, 3500 RPM; MEAN COMPRESSION-SPACE PRESSURE, 4.1 MPa; AVERAGE HEATER-TUBE GAS TEMPERATURE, 690 °C; WORKING GAS, HYDROGEN.

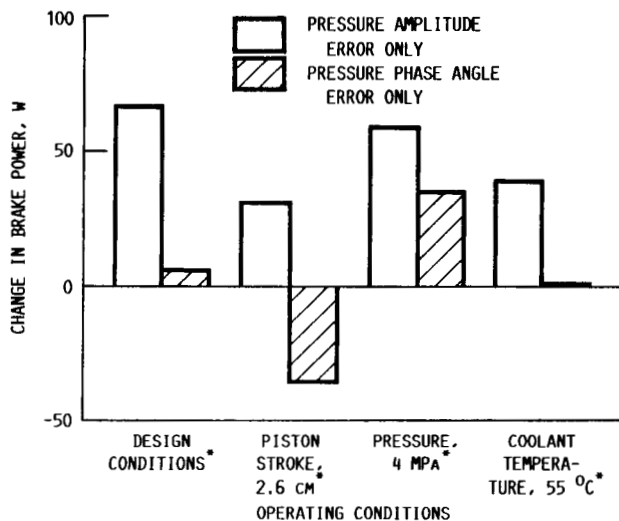


FIGURE 25. - RE-1000 INDICATED POWER SENSITIVITY DUE TO PREDICTION ERRORS IN THE PRESSURE AMPLITUDE OR PHASE ANGLE. DESIGN CONDITIONS; PRESSURE, 7 MPa; PISTON STROKE, 2.6 CM; COOLANT INLET TEMPERATURE, 25 °C; AVERAGE HEATER WALL TEMPERATURE, 600 °C.

*OTHER PARAMETERS HELD AT DESIGN CONDITIONS.



Report Documentation Page

1. Report No. NASA CR-182248 DOE/NASA/4105-4		2. Government Accession No.		3. Recipient's Catalog No.	
4. Title and Subtitle NASA Lewis Stirling Engine Computer Code Evaluation				5. Report Date January 1989	
				6. Performing Organization Code	
7. Author(s) Timothy J. Sullivan				8. Performing Organization Report No. E-4580	
				10. Work Unit No. 778-35-13	
9. Performing Organization Name and Address Sverdrup Technology, Inc. NASA Lewis Research Center Group Cleveland, Ohio 44135-3191				11. Contract or Grant No. NAS3-24105	
				13. Type of Report and Period Covered Contractor Report Final	
12. Sponsoring Agency Name and Address U.S. Department of Energy Office of Vehicle and Engine R&D Washington, D.C. 20545				14. Sponsoring Agency	
				15. Supplementary Notes Prepared under Interagency Agreement DE-AI01-85CE50112. Project Manager, Lanny G. Thieme, Power Technology Division, NASA Lewis Research Center, Cleveland, Ohio 44135.	
16. Abstract In support of the U.S. Department of Energy's Stirling Engine Highway Vehicle Systems program, the NASA Lewis Stirling engine performance code was evaluated by comparing code predictions without engine-specific calibration factors to GPU-3, P-40, and RE-1000 Stirling engine test data. The error in predicting power output was -11 percent for the P-40 and 12 percent for the RE-1000 at design conditions and 16 percent for the GPU-3 at near-design conditions (2000 rpm engine speed versus 3000 rpm at design). The efficiency and heat input predictions showed better agreement with engine test data than did the power predictions. Concerning all data points, the error in predicting the GPU-3 brake power was significantly larger than for the other engines and was mainly a result of inaccuracy in predicting the pressure phase angle. Analysis into this pressure phase angle prediction error suggested that improvements to the cylinder hysteresis loss model could have a significant effect on overall Stirling engine performance predictions.					
17. Key Words (Suggested by Author(s)) Stirling engine Computer predictions			18. Distribution Statement Unclassified - Unlimited Subject Category 44 DOE Category UC-96		
19. Security Classif. (of this report) Unclassified		20. Security Classif. (of this page) Unclassified		21. No of pages 42	22. Price* A03